A voltage-dependent K^+ channel in the lysosome is required for refilling lysosomal Ca^{2+} stores

Wuyang Wang,[1] Xiaoli Zhang,[1] Qiong Gao,[1] Maria Lawas,[1] Lu Yu,[1] Xiping Cheng,[1] Mingxue Gu,[1] Nirakar Sahoo,[1] Xinran Li,[1] Ping Li,[1,2] Stephen Ireland,[1] Andrea Meredith,[3] and Haoxing Xu[1]

[1]Department of Molecular, Cellular, and Developmental Biology, University of Michigan, Ann Arbor, MI 48109
[2]Collaborative Innovation Center of Yangtze River Delta Region Green Pharmaceuticals, College of Pharmaceutical Sciences, Zhejiang University of Technology, Hangzhou 310014, China
[3]Department of Physiology, University of Maryland School of Medicine, Baltimore, MD 21201

The resting membrane potential ($\Delta\psi$) of the cell is negative on the cytosolic side and determined primarily by the plasma membrane's selective permeability to K^+. We show that lysosomal $\Delta\psi$ is set by lysosomal membrane permeabilities to Na^+ and H^+, but not K^+, and is positive on the cytosolic side. An increase in juxta-lysosomal Ca^{2+} rapidly reversed lysosomal $\Delta\psi$ by activating a large voltage-dependent and K^+-selective conductance ($LysoK_{VCa}$). $LysoK_{VCa}$ is encoded molecularly by SLO1 proteins known for forming plasma membrane BK channels. Opening of single $LysoK_{VCa}$ channels is sufficient to cause the rapid, striking changes in lysosomal $\Delta\psi$. Lysosomal Ca^{2+} stores may be refilled from endoplasmic reticulum (ER) Ca^{2+} via ER–lysosome membrane contact sites. We propose that $LysoK_{VCa}$ serves as the perilysosomal Ca^{2+} effector to prime lysosomes for the refilling process. Consistently, genetic ablation or pharmacological inhibition of $LysoK_{VCa}$, or abolition of its Ca^{2+} sensitivity, blocks refilling and maintenance of lysosomal Ca^{2+} stores, resulting in lysosomal cholesterol accumulation and a lysosome storage phenotype.

Introduction

The precise delivery of hydrolases and cargoes to lysosomes for degradation and the timely removal of lysosomal catabolites require the establishment of luminal ionic homeostasis, ionic membrane gradients, and a membrane potential ($\Delta\psi$; Morgan et al., 2011; Mindell, 2012; Xu and Ren, 2015). The lysosomal membrane maintains 1,000- to 5,000-fold concentration gradients for H^+ and Ca^{2+} (Xu and Ren, 2015). It has been established that lysosomal H^+ homeostasis is required for hydrolase activation (Mindell, 2012) and that lysosomal Ca^{2+} efflux mediates signals integral to lysosomal membrane trafficking; however, the lysosomal effectors on which Ca^{2+} acts are largely unknown (Kiselyov et al., 2010; Shen et al., 2012). Several specific ion-dependent channels/transporters have been identified in lysosomes, including the V-ATPase H^+ pump and transient receptor potential mucolipin channels (TRPMLs), the principle Ca^{2+} release channels in the lysosome (Medina et al., 2015; Wang et al., 2015; Xu and Ren, 2015). H^+ channels and Ca^{2+} transporters in the lysosomes, however, remain to be molecularly identified (Xu and Ren, 2015; Garrity et al., 2016).

Much less is understood about the roles of Na^+ and K^+ in lysosomal physiology. Although manipulations of lysosomal Na^+ and K^+ with ionophores can affect several lysosomal functions (Morgan et al., 2011), it was not recognized until recently that, based on ionic composition analysis of isolated lysosomes, there may exist large concentration gradients (>10-fold) across lysosomal membranes for both ions ($[Na^+]_{Lumen} >> [Na^+]_{Cytosol}$, $E_{Na} > 57$ mV; $[K^+]_L << [K^+]_C$, $E_K < -57$ mV; Wang et al., 2012; Xu and Ren, 2015). With these ionic concentration gradients, and based on knowledge extrapolated from plasma membrane studies, resting lysosomal $\Delta\psi$ has been expected to be set by the membrane's relative permeability to K^+ over Na^+ ions (P_K/P_{Na}; Cang et al., 2015; Xu and Ren, 2015). Lysosomal $\Delta\psi$, considered essential for lysosome function (Mindell, 2012), is thought to be negative ($V_{Lumen} = 30$ mV; $V_{Cytosol}$ is defined to 0 mV; $\Delta\psi = V_{Cytosol} - V_{Lumen} = -V_{Lumen} = \sim -30$ mV), which is suggestive of high P_K/P_{Na} in rest conditions. Considering that lysosomal H^+ permeability may also contribute a positive value to lysosomal $\Delta\psi$, background P_K at resting conditions is expected to be even higher to maintain a negative lysosomal $\Delta\psi$. Note that depending on the ratio of $[Cl^-]_L$ versus $[Cl^-]_C$, background P_{Cl} would also contribute a small positive or negative value to lysosomal $\Delta\psi$ (Mindell, 2012).

Recently, we identified two-pore channels (TPCs) as the major Na^+-selective channels in the lysosome that affect $\Delta\psi$ (Wang et al., 2012). Although still controversial, TPCs may also mediate lysosomal Ca^{2+} or H^+ conductance (Patel, 2015). The

Correspondence to Haoxing Xu: haoxingx@umich.edu

Abbreviations used: GPN, glycylphenylalanyl-2-naphthylamide; IBTX, iberiotoxin; KO, knockout; STIM, stromal interaction molecule; TPC, two-pore channel; WT, wild-type.

The Rockefeller University Press $30.00
J. Cell Biol.
https://doi.org/10.1083/jcb.201612123

main goal of the current study was to identify the lysosomal K^+ channels that regulate lysosomal $\Delta\psi$ (Xu and Ren, 2015). During the course of this study, two other research groups reported the existence of K^+-selective channels in the lysosome (Cang et al., 2015; Cao et al., 2015). The functional identification of Na^+- and K^+-selective channels in the lysosome is consistent with the notion that the lysosome lumen is a high Na^+ but low K^+ compartment (Wang et al., 2012; Xu and Ren, 2015). However, our voltage- and current-clamping analyses of isolated lysosomes in the current study suggest that in contrast to previous views, lysosomal $\Delta\psi$ is positive, and background P_K is minimal.

Results

Ubiquitous Ca^{2+}-activated K^+-current in the lysosomes, but not early endosomes

To investigate lysosomal K^+-selective conductances, we performed whole-endolysosome recordings using a high K^+ bath/cytoplasmic solution ($[K^+]_C$ = 140 mM; $[K^+]_L$ = 5 mM; pH_{LY} = 4.6; Fig. 1 A) in various mammalian cell lines and primary cells. In Cos-1 cells, endolysosomes were enlarged from <0.5 to ≤5 µm with vacuolin-1 (Dong et al., 2008). Vacuolin-1 selectively enlarged endosomes and lysosomes, but not other intracellular organelles such as mitochondria or ER (Cerny et al., 2004). Although EEA1-positive early endosomes were also slightly enlarged, only Lamp1-positive vacuoles were enlarged to patchable sizes (Fig. S1 A). Enlarged vacuoles were then isolated and patch-clamped (Dong et al., 2008; Wang et al., 2012). Negligible or no outward currents (<50 pA at 120 mV) were seen in most vacuoles, suggesting that the background TMEM175-like K^+ conductance reported by Cang et al. (2015) under high luminal K^+ and pH recording conditions is minimally active under our experimental conditions. However, increasing the concentration of Ca^{2+} from the bath/cytoplasmic side ($[Ca^{2+}]_C$) to 100–1,000 µM induced the rapid appearance of large (>200 and ≤3,000 pA at 120 mV) outwardly rectifying currents (Fig. 1, B and C). Similar Ca^{2+}-activated outward currents were detected in endolysosomes enlarged spontaneously (Dong et al., 2010), by sucrose treatment (Bandyopadhyay et al., 2014), or by apilimod treatment (Cai et al., 2014; Fig. S1 B). In contrast, Ca^{2+}-activated outward currents were not detected in isolated early endosomes, which could be artificially enlarged by either overexpression of a dominant-negative Rab5 mutant (Rab5-Q79L) in the cells (Wegner et al., 2010) or pretreatment with vicenistatin (Nishiyama et al., 2016; Fig. 1, D and E; and Fig. S1 C), suggesting the lysosome specificity of the currents.

Substitution of luminal Cl^- with gluconate$^-$, which largely abolished the background outwardly rectifying Cl^- currents seen in some patches, did not affect the Ca^{2+}-activated outward currents, suggesting that the currents were mediated by influx of K^+ into the luminal side (Fig. 1 F). Consistent with this interpretation, replacement of K^+ with Na^+ or Cs^+ in the bath solution abolished the currents completely (Fig. 1 G). Because current activation is also strongly dependent on membrane voltage (Fig. 1, B, F, and G), we define this Ca^{2+}-activated current as the lysosomal voltage- and Ca^{2+}-activated K^+ current ($LysoK_{VCa}$). Notably, $LysoK_{VCa}$ was noisy (Fig. 1, B, F, and G), as is characteristic of channels with high unitary conductance. $LysoK_{VCa}$ was detected ubiquitously in various mammalian cell types, including HEK293T cells, CV1 monkey kidney cells, A7r5 smooth muscle cells, INS-1 pancreatic cells, primary mouse cortical neurons, mouse bladder epithelial cells (BECs), mouse embryonic fibroblasts (MEFs), and mouse parietal cells (Fig. 2, A and D; and Fig. S2, A–F and J).

$LysoK_{VCa}$ is mediated by SLO1

$LysoK_{VCa}$ resembles the BK (maxi-K) currents at the cell surface of excitable cells, such as muscle cells and neurons (Shi et al., 2002; Salkoff et al., 2006; Yuan et al., 2010). BK channels are formed by the coassembly of the pore-forming SLO1 (KCNMA1) subunit and auxiliary β (KCNMB1–4) or γ subunits (Salkoff et al., 2006; Yuan et al., 2010). Unlike wild-type (WT) MEFs, in the KCNMA1 knockout (KO) MEFs (Fig. S2 I), no $LysoK_{VCa}$-like currents were seen (Fig. 2, A, B, and D). Likewise, $LysoK_{VCa}$ currents were detected in WT but not KCN MA1 KO mouse parietal cells (Figs. 2 D and S2 J). In contrast, endogenous, background, whole-cell K^+-selective outward currents were not different between WT and KCNMA1 KO MEF cells (Fig. S2 K). It should be noted that the plasma membrane background K^+ conductances (Fig. S2 K), which are known to set the resting membrane potential of the cell, were undetectable in the lysosomes of KCNMA1 KO cells (Fig. 2, B and D; and Fig. S2 I), suggesting that BK channels are uniquely targeted to lysosomes.

On the other hand, overexpression of mouse SLO1-YFP (YFP tag is in the cytoplasmic side) or human SLO1-GFP in Cos-1 cells resulted in large $LysoK_{VCa}$-like currents, even under basal conditions ($[Ca^{2+}]_C$ = 0.1 µM; Fig. 2, C and D), and those currents could be augmented further by increasing cytoplasmic Ca^{2+} (Fig. 2 C). In contrast, overexpression of other K_V channels (e.g., K_V2.1-GFP) failed to increase whole-endolysosomal K^+ currents. Collectively, these results suggest that SLO1 proteins are the molecular mediators of $LysoK_{VCa}$.

SLO1 has been observed in intracellular organelles, including the nucleus and mitochondria, of excitable cells in addition to the plasma membrane (Singh et al., 2012, 2013; Li et al., 2014). Organelle fractionation analysis revealed that SLO1-YFP proteins (splicing variants containing the VEDEC sequence; Singh et al., 2013) in transfected Cos-1 cells were enriched in both Lamp1-resident lysosomal fractions and complex II–resident mitochondrial fractions (Fig. 2 E). Furthermore, fluorescence analysis showed that overexpressed SLO1 proteins were localized predominantly in the Lamp1-positive late endosomal and lysosomal compartments (Fig. 2, F and G). In contrast, under the same microscopic settings, SLO1 was rarely colocalized to a significant degree with markers for nuclear membranes, early endosomes, ER, Golgi apparatus, or even the plasma membrane, although partial colocalization was also observed for mitochondrial markers (Fig. 2, F and G; and Fig. S2 L). Intriguingly, although large whole-cell BK currents can be measured (Fig. S4 G), in nonexcitable cells, plasma membrane localization of overexpressed SLO1 proteins could be detected only with the aid of surface-specific labeling (Liu et al., 2014). Collectively, these results suggest that, consistent with electrophysiological analyses, the localized, high levels of SLO1 protein expression in lysosomal membranes gives rise to $LysoK_{VCa}$. Dileucine motifs could be responsible for specific targeting of SLO1 proteins to lysosomes (Cao et al., 2015). However, mutations in these motifs did not significantly decrease SLO1-mediated lysosomal (Lyso-SLO1) currents in our hands (Fig. S2, M and N).

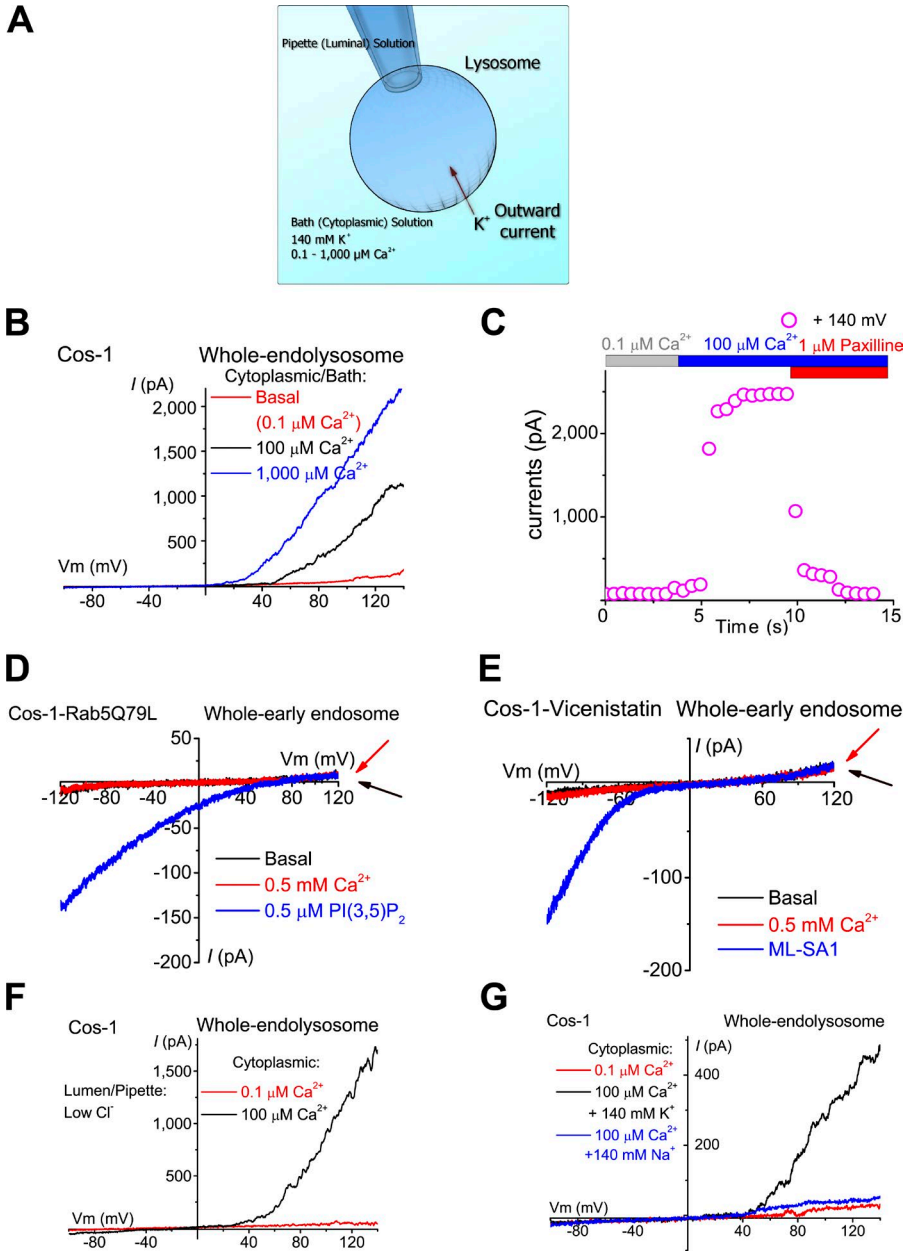

Figure 1. **Ca^{2+}-activated K^+ currents were detected in lysosomes, but not in early endosomes.** (A) Whole-endolysosome patch-clamp configuration. The pipette (extracellular/luminal) solution was a standard Na^+-based external solution (Tyrode's) adjusted to pH 4.6 to mimic the acidic environment of the lysosome lumen. The bath (internal/cytoplasmic) solution was a K^+-based solution (140 mM K^+) with free [Ca^{2+}] ranging from 0.1 to 1,000 µM as indicated in each experiment. The arrow indicates the direction of K^+ ion flow into the endolysosome (defined as the outward current). (B) Bath application of 100 or 1,000 µM Ca^{2+} activated outwardly rectifying currents in an enlarged vacuole from a Cos-1 cell pretreated with vacuolin-1. The currents were elicited by repeated voltage ramps (−100 to 140 mV; 400 ms; only partial voltage ranges are shown) with a 4-s interramp interval. (C) Time courses of current activation by Ca^{2+} in an enlarged vacuole isolated from a Cos-1 cell. (D and E) In isolated early endosomes that were enlarged by Rab5-Q79L overexpression (D) or vicenistatin (E), Ca^{2+} (500 µM) failed to activate measurable whole-endosome outward currents. $PI(3,5)P_2$ (0.5 µM) or ML-SA1 (20 µM) readily activated TPC-like (D) or ML1-like (E) currents, respectively. (F) Representative traces of Ca^{2+}-activated outward currents with a pipette/luminal solution containing low [Cl^-] (11 mM versus 156 mM in G. (G) Substitution of cytoplasmic K^+ with Na^+ abolished Ca^{2+}-activated outward currents.

Dual activation of LysoK$_{VCa}$ by Ca^{2+} and voltage

A unique gating property of BK channels is their dual activation by membrane voltage and cytoplasmic Ca^{2+} (Salkoff et al., 2006). Whole-endolysosomal currents elicited by voltage steps revealed that increasing [Ca^{2+}]$_C$ from basal levels (0.1 µM) to 100–1,000 µM activated outwardly rectifying currents robustly at positive voltages (Figs. 3 A and S3 A). Consistent with LysoK$_{VCa}$'s K^+ selectivity, the Ca^{2+}-activated step currents had an E_{rev} of less than −60 mV under physiology-mimicking recording conditions (calculated E_K = −85.6 mV) and an E_{rev} of ~0 mV under symmetric K^+ solutions.

In SLO1-YFP–expressing Cos-1 cells, whole-endolysosome LysoK$_{VCa}$ step currents were observed in basal Ca^{2+} level conditions at voltages that were less positive than in non-transfected cells (Figs. 3 B and S3 B). An analysis of normalized conductance–voltage curves revealed significant leftward shifts in half-maximal activation voltage ($V_{0.5}$) when [Ca^{2+}]$_C$ was increased in the range of 3–100 µM (Fig. S3, C and D). Similar to BK channels (Yang et al., 2008), cytoplasmic Mg^{2+} activated LysoK$_{VCa}$ and Lyso-SLO1 channels, but blocked the conductance (Fig. S3, F–H).

LysoK$_{VCa}$ exhibits a high single-channel conductance

Consistent with our whole-endolysosome recordings, in a subset of large-sized cytoplasmic-side-out endolysosomal patches, increasing [Ca^{2+}]$_C$ induced robust large-amplitude single-channel openings of LysoK$_{VCa}$ (Fig. 3 C), with a half-maximal concentration (EC_{50}) of ~20 µM at 80 mV (Fig. S3 D). These results suggest that small changes in local juxta-lysosomal Ca^{2+} could readily activate LysoK$_{VCa}$. Single-channel LysoK$_{VCa}$ currents were occasionally seen in small-sized lysosomal patches from SLO1-expressing Cos-1 cells (Fig. S3 E), which typically displayed large macroscopic currents (Fig. 3 D). At 100 µM [Ca^{2+}]$_C$, the channel open

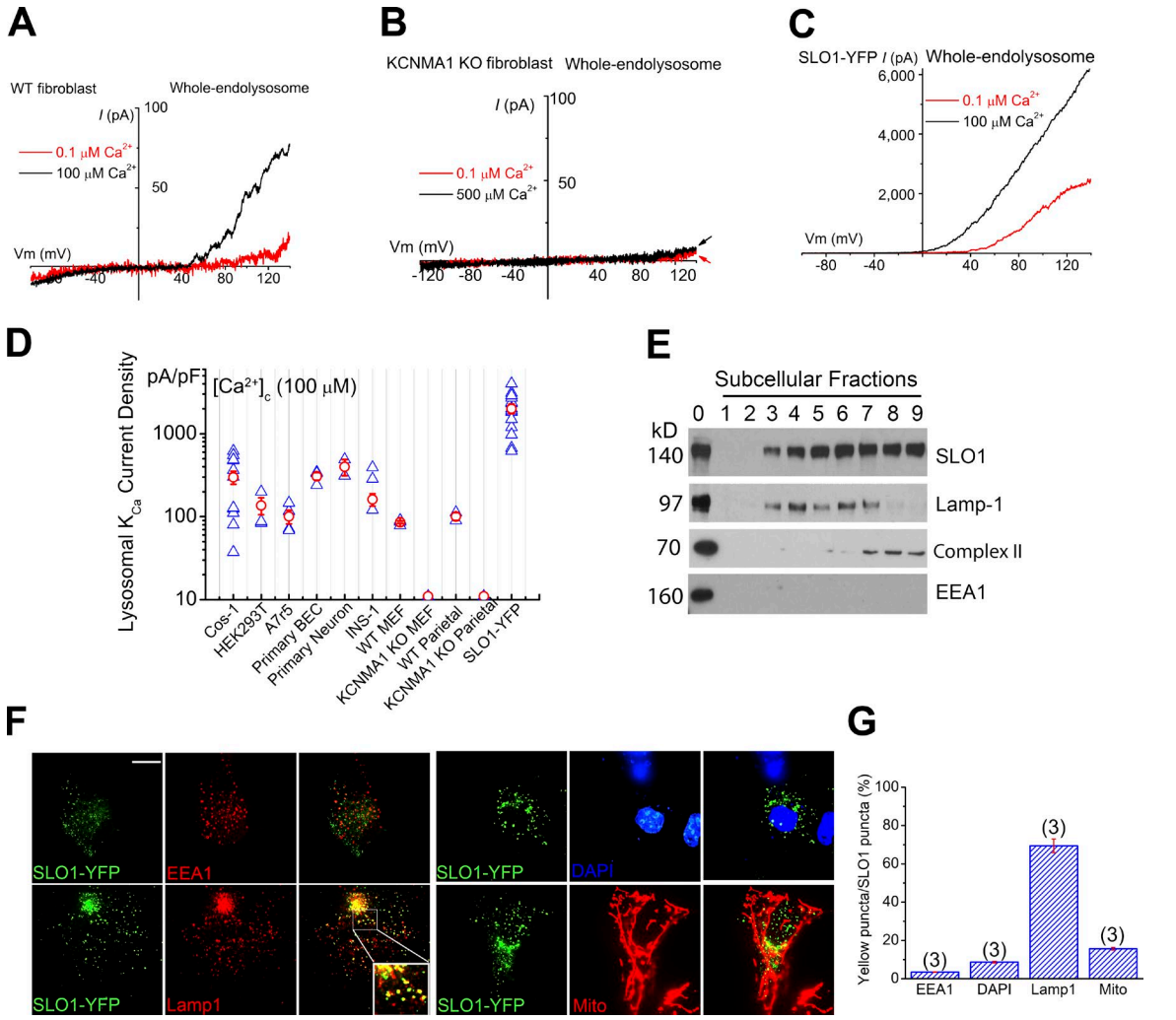

Figure 2. **SLO1 mediates Ca^{2+}-activated K^+ currents in the lysosomes of excitable and nonexcitable cells.** (A) Whole-endolysosome Ca^{2+}-activated outward currents in a WT MEF. (B) Whole-endolysosome Ca^{2+}-activated outward currents in a KCNMA1 KO (*Kcnma1*$^{-/-}$ or *Slo1*$^{-/-}$) MEF. Note the lack of background outward currents typically seen in whole-cell recordings. (C) Whole-endolysosome Ca^{2+}-activated currents in a SLO1-YFP–expressing Cos-1 cell (Lyso-SLO1). (D) Summary of whole-endolysosome Ca^{2+}- and voltage-activated K^+ currents (LysoK_{VCa}) in a variety of cell types, including Cos-1 cells, HEK293T cells, A7r5 smooth muscle cell lines, mouse BECs, cultured mouse cortical neurons, INS-1 pancreatic cell lines, WT and KCNMA1 KO MEFs, WT and KCNMA1 KO parietal cells, and SLO1-YFP-expressing Cos-1 cells. Both individual (blue) and mean (red; ± SEM) current densities are shown for each cell type (n = 3–15 patches). (E) Subcellular fractionation analysis revealed enrichment of SLO1 proteins in organellar fractions containing Lamp-1 or Complex-II (a mitochondrial marker). Subcellular fractionations (1–9) were obtained by gradient-based ultracentrifugation. Cell lysates were included as controls (fraction 0). (F and G) Colocalization analyses of SLO1-YFP with Lamp1, MitoTracker, EEA1 (an early endosomal marker), and DAPI (a nuclear marker). Bar, 10 µm. Error bars indicate SEM.

probability (P_{open}) of LysoK_{VCa} displayed strong voltage dependence (Figs. 3 E and S3 E). In symmetric K^+ solutions, the single-channel conductances for LysoK_{VCa} and Lyso-SLO1 were 231 ± 61 and 219 ± 59 pS (n = 3), respectively (Figs. 3 F and S3 I). Hence, LysoK_{VCa} conducts K^+ efficiently with a large conductance.

Pharmacological and physiological modulation of LysoK_{VCa}

Both LysoK_{VCa} and Lyso-SLO1 exhibited pharmacological properties similar to those of BK channels. Paxilline, a relatively specific membrane-permeable BK inhibitor (Salkoff et al., 2006), inhibited LysoK_{VCa} and Lyso-SLO1 completely (Figs. 3 G and S4, A and E). Quinidine and clofilium, membrane-permeable BK inhibitors with lower specificity than paxilline (Tang et al., 2010), also inhibited both LysoK_{VCa} and Lyso-SLO1 (Figs. 3 H and S4, B and E). Likewise, in the luminal-side-out patches, iberiotoxin (IBTX), a membrane-impermeable BK-specific toxin inhibitor (Tang et al., 2010), completely inhibited single LysoK_{VCa} currents (Fig. 3 I). Conversely, NS1619 (Olesen et al., 1994) and isopimaric acid (Yamamura et al., 2001), BK-specific channel openers, augmented LysoK_{VCa} (Fig. S4, C–E).

Both luminal and cytoplasmic pH are critical determinants of lysosomal physiology (Xu and Ren, 2015). Interestingly, an elevation of lysosomal pH_L from 4.6 to 7.4 markedly enhanced the Ca^{2+} activation of Lyso-SLO1 (Fig. S4, F–H). On the other hand, acidic pH_C readily activated LysoK_{VCa} at basal Ca^{2+} levels (Fig. S4, I–K). These results suggest that under physiological conditions, lysosomal H^+ release may activate LysoK_{VCa} by simultaneously raising luminal pH and decreasing juxta-lysosomal pH.

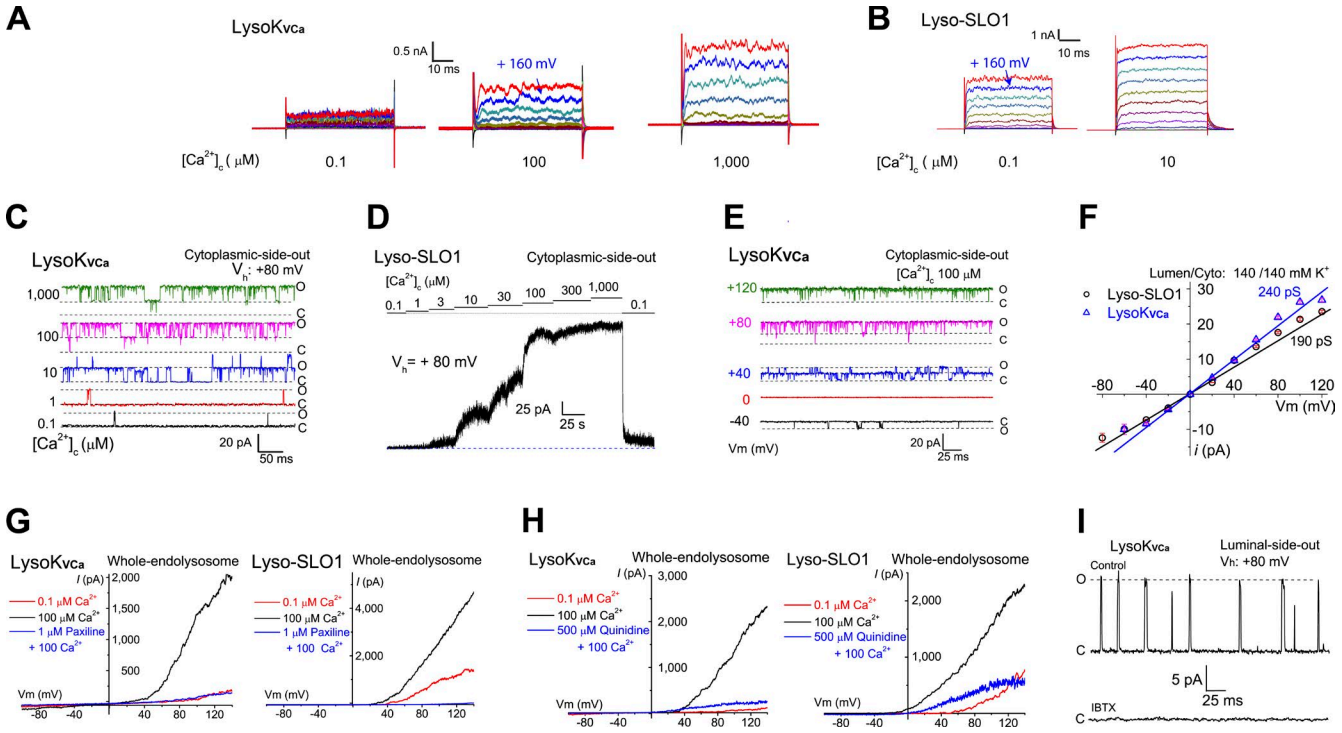

Figure 3. **LysoK$_{VCa}$ is a lysosomal large-conductance K$^+$ channel that is dually activated by Ca^{2+} and voltage.** (A) LysoK$_{VCa}$ currents were activated by cytoplasmic Ca^{2+} ([Ca^{2+}]$_C$; 0.1, 100, and 1,000 µM). After a 20-ms prepulse at −60 mV, currents were elicited by voltage steps from −80 to 180 mV in 20-mV increments. (B) Activation of Lyso-SLO1 by Ca^{2+} and voltage steps. (C) [Ca^{2+}]$_C$-dependent single-channel LysoK$_{VCa}$ currents from a cytoplasmic-side-out patch. The open and closed states are indicated by O and C, respectively. (D) [Ca^{2+}]$_C$ dependence of macroscopic Lyso-SLO1 currents. (E) Voltage-dependent openings of single LysoK$_{VCa}$ channels at [Ca^{2+}]$_C$ of 100 µM in a cytoplasmic-side-out patch with symmetric (luminal/cytoplasmic) K$^+$ (140 mM) solutions. (F) Unitary single-channel chord conductances of LysoK$_{VCa}$ and Lyso-SLO1. (G) LysoK$_{VCa}$ and Lyso-SLO1 currents were blocked by the BK-specific inhibitor paxilline (1 µM). (H) Quinidine (500 µM), a SLO1/SLO3 channel inhibitor, blocked LysoK$_{VCa}$ and Lyso-SLO1 currents. (I) Single LysoK$_{VCa}$ currents were inhibited by bath application of 100 nM IBTX to a luminal-side-out patch.

Regulation of LysoK$_{VCa}$ by auxiliary subunits and trafficking

The functional diversity of BK channels can be conferred by cell type–specific or location-specific assembly of SLO1 with various auxiliary β and γ subunits (Yan and Aldrich, 2010; Hoshi et al., 2013). For example, β2 and a subset of β3 isoforms are known to confer fast and voltage-dependent inactivation of BK currents, respectively, in both heterologous expression and endogenous settings (Zeng et al., 2001; Xia et al., 2003; Torres et al., 2014). Notably, overexpression of β2-GFP together with SLO1 resulted in fast-inactivating Lyso-SLO1 currents (Fig. 4 A). In INS-1 cells, which express β3 subunits (Braun et al., 2008; Torres et al., 2014), and cultured BECs, LysoK$_{VCa}$ exhibited voltage-dependent inactivation or blockage at high voltages (Fig. S2, D and E, and Fig. S5 A). Notably, heterologously expressed β subunits, including β2, were found to be localized in Lamp1-positive compartments (Figs. 4 B and S5 B).

We examined whether endogenous SLO1 proteins are present at the plasma membrane of LysoK$_{VCa}$-expressing non-excitable cells. In Cos-1 cells, measurable whole-cell paxilline- and IBTX-sensitive BK-like currents were detected (Fig. 4 C and Fig. S5, C–F), but the current density was, at most, a tenth of that of LysoK$_{VCa}$ (Fig. 4 D). Consistently, in MEFs, no measurable whole-cell BK-like currents were detected (Figs. 4 D and S5 G). Hence, in nonexcitable cells, SLO1 proteins may be preferentially or specifically targeted to lysosomes where they mediate LysoK$_{VCa}$.

Regulation of lysosomal membrane potential by Ca^{2+} and LysoK$_{VCa}$

In excitable cells, BK acts as a negative-feedback regulator of membrane excitability (Salkoff et al., 2006). To investigate the role of LysoK$_{VCa}$ in regulating lysosomal excitability, we performed current-clamp recordings on isolated enlarged endolysosomes. Lysosomal Δψ (i.e., $V_{Cytosol} - V_{Lumen} = -V_{Lumen}$, because $V_{Cytosol}$ is defined to 0 mV; Fig. 5, A and B) is thought to be negative (approximately −30 mV; Morgan et al., 2011). Under our experimental conditions (high lysosomal Na$^+$ and low lysosomal K$^+$; Wang et al., 2012; Fig. 5, A and B), direct electrophysiological measurement revealed that Δψ was in fact positive (15–30 mV; Fig. 5, C–F). Removal of either luminal Na$^+$ or H$^+$ reduced Δψ by ∼15–20 mV, whereas removal of both ions simultaneously caused a reversal of Δψ to approximately −30 mV (Fig. 5 D). Similarly, bath application of the K$^+$ ionophore valinomycin (Van Dyke, 1995) also reversed lysosomal Δψ (Fig. 5 C), suggesting a limited K$^+$ permeability at rest conditions and, in contrast to the plasma membrane, an increase of K$^+$ permeability in the lysosome that would result in a large change of lysosomal Δψ. Conversely, bath application of H$^+$ ionophores niclosamide (Fonseca et al., 2012) or activation of TPCs with PI(3,5)P$_2$ (Wang et al., 2012) caused a further positive shift in Δψ (Fig. 5, C and J). In the absence of PI(3,5)P$_2$, inclusion of ATP in the bath solution had a minimal effect on lysosomal Δψ (Fig. 5 E). Together, these results suggest that in the enlarged lysosomes, the primary determinants of "resting" lysosomal Δψ are the lysosomal membrane's Na$^+$ and H$^+$ per-

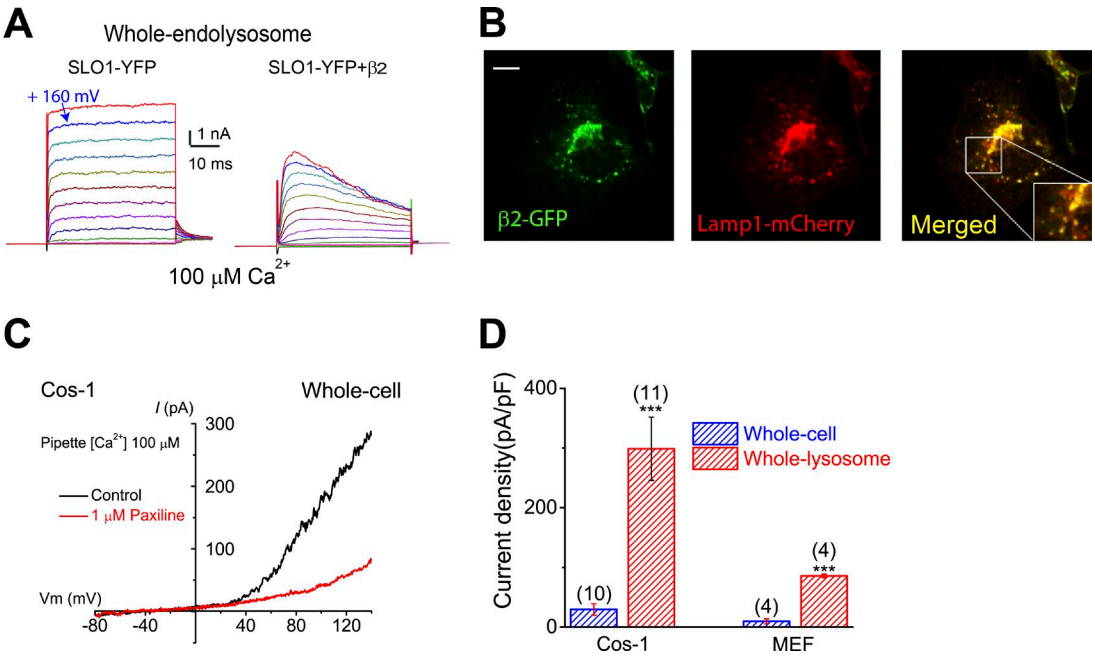

Figure 4. **Lysok$_{VCa}$ is preferentially expressed in the lysosome.** (A) Step currents of Lyso-SLO1 (left) and Lyso-SLO1+ β2 (right) in the presence of 100 μM Ca^{2+}. (B) Localization of β2-GFP in the Lamp1-positive compartments. Bar, 10 μm. (C) Whole-cell K^+ currents sensitive to paxilline (1 μM) in nontransfected Cos-1 cells. The pipette solution contained 100 μM Ca^{2+}. (D) Densities (mean ± SEM) of plasma membrane BK-like currents vs. Lysok$_{VCa}$ in Cos-1 cells and MEFs. Statistical comparisons were made with variance analysis (Student's *t* test). ***, P < 0.001.

meabilities under our experimental conditions (Fig. 5 D), but not its K^+ permeability, as the lysosomal Δψ is positive in its value. Even at neutral pH, lysosomal Δψ is slightly positive (Fig. 5 D), suggesting that resting P_{Na} is slightly higher than resting P_K.

Notably, increasing cytoplasmic Ca^{2+} reduced lysosomal Δψ (Fig. 5, F and J; see also Fig. 5, A and B). Indeed, in small-sized vacuoles with only single Lysok$_{VCa}$ channel openings (Fig. S5 H), rapid and transient paxilline-sensitive decreases in lysosomal Δψ were observed (Fig. 5 G). Overexpression of SLO1 (Fig. S5, I–K) also resulted in reduced Δψ (Fig. 5, H and J). Furthermore, in endolysosomes expressing gain-of-function mutant SLO1 (SLO1^{R207Q}) channels (Montgomery and Meredith, 2012), which exhibited large basal currents at less positive voltages (Fig. S5, J–L), lysosomal Δψ was reversed to −20 to approximately −30 mV (Fig. 5, I and J). In SLO1- or SLO1^{R207Q}-expressing vacuoles, increasing cytoplasmic Ca^{2+} resulted in a much more negative lysosomal Δψ (−60 mV; Fig. 5, H–J). Collectively, these results suggest that Lysok$_{VCa}$ regulates lysosomal Δψ in response to changes in juxta-lysosomal Ca^{2+} levels.

Lysosomal K^+ homeostasis and cytosolic Ca^{2+} increase are both required for lysosomal Ca^{2+} store refilling

Lysosomal Δψ is a critical determinant of lysosomal ion homeostasis, including Ca^{2+} homeostasis, which is maintained at a luminal concentration of ∼0.5 mM (Morgan et al., 2011; Xu and Ren, 2015). To investigate the molecular mechanisms that regulate lysosomal Ca^{2+} stores, we recently developed a lysosomal Ca^{2+} refilling assay using ML-SA1, a membrane-permeable synthetic activator of lysosomal TRPML1 (or ML1) channels (Shen et al., 2012). In HEK293 cell lines stably expressing GCaMP3-ML1 (Fig. 6 A; HEK-GCaMP3-ML1 cells), bath application of ML-SA1 in a zero (<10 nM) Ca^{2+} external solution produced robust lysosomal Ca^{2+} release indicated by GCaMP3 fluorescence (Garrity et al., 2016). After 3–5 min of refilling time, secondary ML-SA1 responses were largely recovered (Fig. 6 B), suggesting that lysosomal Ca^{2+} stores were refilled (Garrity et al., 2016). Using this refilling assay, we recently reported that in contrast to previous findings, dissipating the H^+ gradient does not block lysosomal Ca^{2+} refilling (Garrity et al., 2016). Instead, ER Ca^{2+} may refill lysosomal Ca^{2+} stores, via the presumed formation of ER–lysosome membrane contacts (Eden, 2016). Remarkably, dissipating the lysosomal K^+ gradient with valinomycin resulted in a blockade of lysosomal Ca^{2+} store filling (Fig. 6, C and D; and Fig. S6 A), suggesting an essential role of lysosomal K^+ gradient and efflux in refilling.

In theory, either a reduction in luminal Ca^{2+} or an increase in perilysosomal Ca^{2+} could serve as a trigger for Ca^{2+} refilling. Cytoplasmic Ca^{2+} increases have been hypothesized to regulate the formation and stabilization of ER–lysosome membrane contacts (Eden, 2016; Kilpatrick et al., 2017), potentially contributing to lysosomal Ca^{2+} refilling. To investigate the second possibility, we used a complementary refilling assay, based on the use of Oregon Green 488 Bapta-1-dextran (OG-BAPTA) dyes to directly measure lysosomal luminal Ca^{2+} contents (Garrity et al., 2016). Notably, chelating cytosolic Ca^{2+} completely blocked refilling (Fig. 6, E and F).

Lysok$_{VCa}$ is required for efficient lysosomal Ca^{2+} store refilling in normal physiology

We next tested the hypothesis that Lysok$_{VCa}$ mediates Ca^{2+}-activated K^+ permeability that participates in perilysosomal Ca^{2+}-triggered lysosomal refilling. Remarkably, in the GCaMP-based refilling assays, when we inhibited Lysok$_{VCa}$ acutely using membrane-permeable BK inhibitors (i.e., paxilline and quinidine) during refilling, lysosomal Ca^{2+} refilling was completely inhibited (Fig. 7, A–C). In contrast, refilling was not

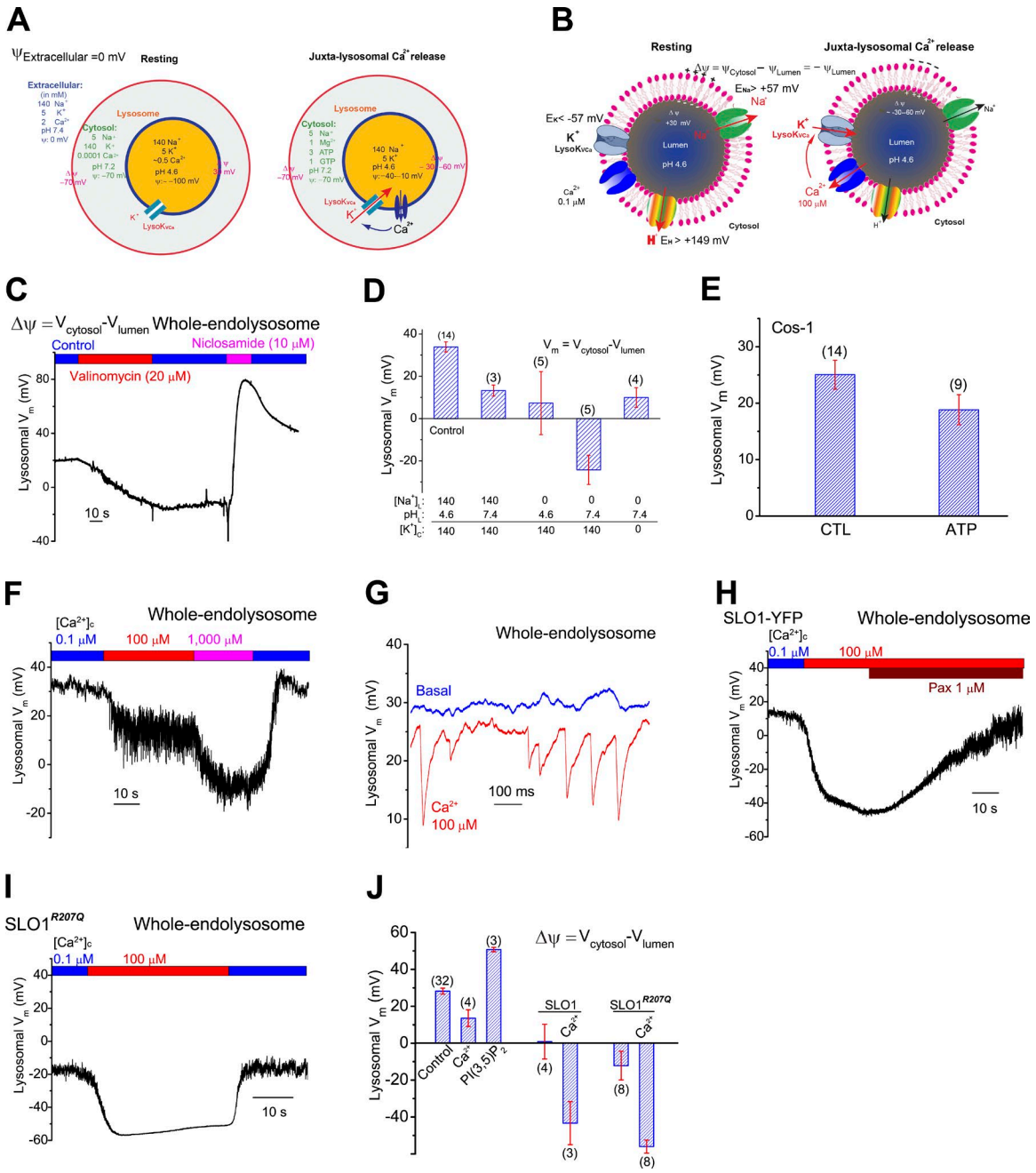

Figure 5. **Regulation of lysosomal membrane potential by lysosomal K⁺ and LysoK$_{VCa}$.** (A) When the voltage or potential (ψ) of the extracellular solution is set to 0 mV by conventional definition, the ψ of the cytosol ($\psi_{Cytosol}$) is approximately −70 mV. Hence the resting membrane potential (Δψ) of the cell is approximately −70 mV (cytoplasmic-side negative). At resting conditions, ψ_{Lumen} is −100 mV and lysosomal Δψ ($\psi_{Cytosol} - \psi_{Lumen}$) is 30 mV. Upon activation of LysoK$_{VCa}$, depending on the extent of LysoK$_{VCa}$ activation, lysosomal Δψ is reversed to −30 to −60 mV. (B) When $\psi_{Cytosol}$ is set to 0 mV, lysosomal Δψ at rest is 30 mV. Assuming >10-fold concentration gradients across lysosomal membranes for Na⁺ and K⁺ ($[Na^+]_L >> [Na^+]_C$ and $[K^+]_L << [K^+]_C$), E_{Na} is >57 mV and E_K is <−57 mV. Likewise, E_H is >149 mV. The resting Δψ is determined primarily by Na⁺ and H⁺ permeabilities. Upon Ca^{2+} activation of LysoK$_{VCa}$, lysosomal Δψ is changed to −30 to −60 mV. (C) Effects of K⁺ (valinomycin) and H⁺ (niclosamide) ionophores on lysosomal Δψ in a Cos-1 cell in a current-clamp vacuole. (D) Summary of lysosomal Δψ under different ionic compositions in the luminal and cytoplasmic sides. Lysosomal Δψ was 20 – 30 mV under control conditions (lumen, 145 mM Na⁺, pH 4.6; cytosol, 140 mM K⁺, pH 7.4). Replacement of luminal Na⁺ with NMDG⁺ or increasing luminal pH from 4.6 to 7.4 led to a reduction in Δψ. (E) Resting lysosomal Δψ with or without ATP in the bath/cytoplasmic solutions. (F) Current-clamp recordings of lysosomal Δψ in a Cos-1 cell. (G) $[Ca^{2+}]_C$ (100 μM) induced voltage transients in a current-clamped vacuole. Single-channel LysoK$_{VCa}$ currents from the same vacuole under the voltage-clamp configuration are shown in Fig. S5 H. (H and I) Lysosomal Δψ in enlarged vacuoles from SLO1-YFP-expressing (H) and SLO1^{R207Q}-expressing (I) cells. LysoK$_{VCa}$ currents from the same patches under the voltage-clamp configuration are shown in Fig. S5, K and L. (J) Summary of lysosomal Δψ in various conditions. In D, E, and J, means ± SEM are shown.

affected by IBTX (a membrane-impermeable BK inhibitor) or NS1619 (a membrane-permeable BK opener; Fig. S6, D and E). Prolonged inhibition (3 h) of LysoK$_{VCa}$ abolished the naive Ca^{2+} release responses (Fig. S6, B, C, and E), suggesting that refilling is an ongoing process with constitutive Ca^{2+} release in the cells (Garrity et al., 2016). Note that paxilline did not directly

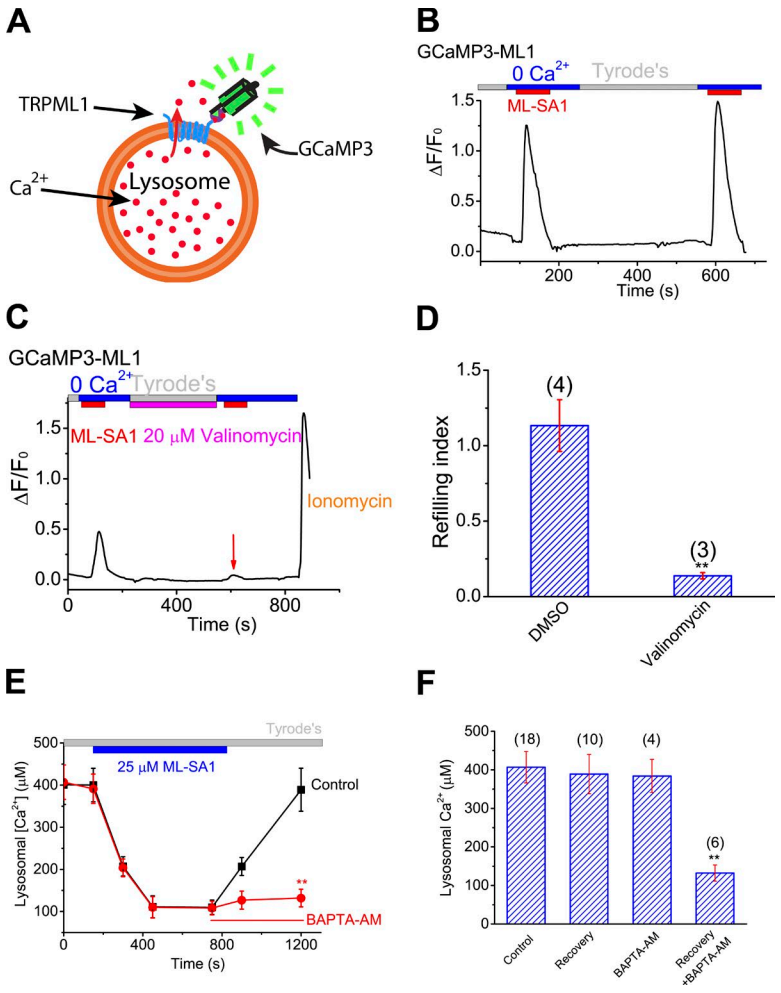

Figure 6. **Lysosomal K^+ homeostasis and cytosolic Ca^{2+} increase are both required for lysosomal Ca^{2+} store refilling.** (A) Lysosome-targeted genetically encoded Ca^{2+} indicator GCaMP3-ML1. (B) In HEK293 cells stably expressing GCaMP3-ML1 (HEK-GCaMP3-ML1 cells), lysosomal Ca^{2+} release, as indicated by elevated GCaMP3 fluorescence (F_{470}), was induced by bath application of ML-SA1 (25 μM), a membrane-permeable ML1-specific agonist, in a 0 Ca^{2+} (<10 nM) external solution. Averaged responses of 15–30 cells in one coverslip are shown. (C) Short-term (5-min) application of valinomycin (20 μM) in the refilling phase abolished the second ML-SA1 response. (D) Effect of valinomycin on lysosome Ca^{2+} refilling. (E and F) Effect of BAPTA-AM treatment on recovery of lysosomal Ca^{2+} content upon ML-SA1 treatment in ML1-expressing HEK293 cells that were loaded with OG-BAPTA dextran dyes. Statistical comparisons were made with variance analysis (Student's *t* test). **, $P < 0.01$. Error bars indicate SEM.

affect the activity of lysosomal ML1 channels (Fig. S6, F and J) or luminal pH (Fig. S6, H and I).

Consistently, when $LysoK_{VCa}$ was genetically inactivated, as was seen in GCaMP7-ML1–transfected KCNMA1 KO MEFs, lysosomal Ca^{2+} refilling was also significantly reduced, but not abolished compared with WT MEFs (Fig. 7, D and G). Heterologous expression of WT SLO1-mCherry largely restored lysosomal refilling in KCNMA1 KO MEFs (Fig. 7, F and G). In contrast, when the Ca^{2+}-sensitivity of SLO1-mCherry was abolished by mutations ($SLO1^{M513I/D898A}$) in the Ca^{2+}-binding sites (Bao et al., 2004; Fig. 7 E), the restoration effect was lost (Fig. 7, F and G). Hence, Ca^{2+} activation of $LysoK_{VCa}$ is specifically required for refilling of lysosomal Ca^{2+} stores.

To further investigate the role of $LysoK_{VCa}$ in regulating lysosomal Ca^{2+} store refilling, we studied refilling in cells loaded with Fura-2 using glycylphenylalanyl-2-naphthylamide (GPN), a lysosome-specific reagent that is widely used to deplete lysosomal Ca^{2+} stores (Berg et al., 1994), to induce ML1-independent Ca^{2+} release from lysosomes (Garrity et al., 2016). Blocking $LysoK_{VCa}$ in the refilling phase by using paxilline markedly attenuated the refilling response in both HEK293 cells and WT MEFs (Fig. 7, H–J; and Fig. S6, K–M) but had no effect on the residual refilling response observed in KCNMA1 KO MEFs (Fig. 7 J). It is of note that the naive ML-SA1– or GPN-induced Ca^{2+} release responses in the KCNMA1 KO cells or WT cells treated with paxilline acutely were comparable to those in nontreated WT cells (Fig. 7, D and H). Likewise, no difference was noted between WT and KCNMA1 KO cells in the OG-BAPTA assay (Fig. 8). Hence, $LysoK_{VCa}$ is not required for ML1-mediated lysosomal Ca^{2+} release per se.

The recovery of lysosomal Ca^{2+} contents was profoundly inhibited by paxilline treatment in WT MEFs (Fig. 8, A and B). In contrast, the partial recovery seen in KCNMA1 KO MEFs was completely insensitive to paxilline (Fig. 8, A and B). Furthermore, overexpressing SLO-mCherry, but not $SLO1^{M513I/898A}$-mCherry, in KCNMA1 KO MEFs largely rescued the refilling of lysosomal Ca^{2+} contents (Fig. 8 C). Finally, pretreatment with paxilline dramatically decreased lysosomal Ca^{2+} contents in WT MEFs but had no effect on lysosomal Ca^{2+} stores or refilling in KCNMA1 KO MEFs (Fig. 8 D). Collectively, these results suggest that although there exist compensatory mechanisms for lysosomal store refilling in cells lacking KCNMA1, $LysoK_{VCa}$ is required for efficient refilling of lysosomal Ca^{2+} stores in normal physiology.

Genetic ablation or pharmacological inhibition of $LysoK_{VCa}$ leads to lysosomal dysfunction

Lysosomal Ca^{2+} and $\Delta\psi$ are important for lysosomal function (Medina et al., 2015; Wang et al., 2015; Xu and Ren, 2015). Lysosomal dysfunction is commonly associated with a compensatory increase in lysosome biogenesis, manifested as increased expression of essential lysosomal genes (Xu and Ren, 2015). For example, the expression of Lamp1, a housekeeping gene

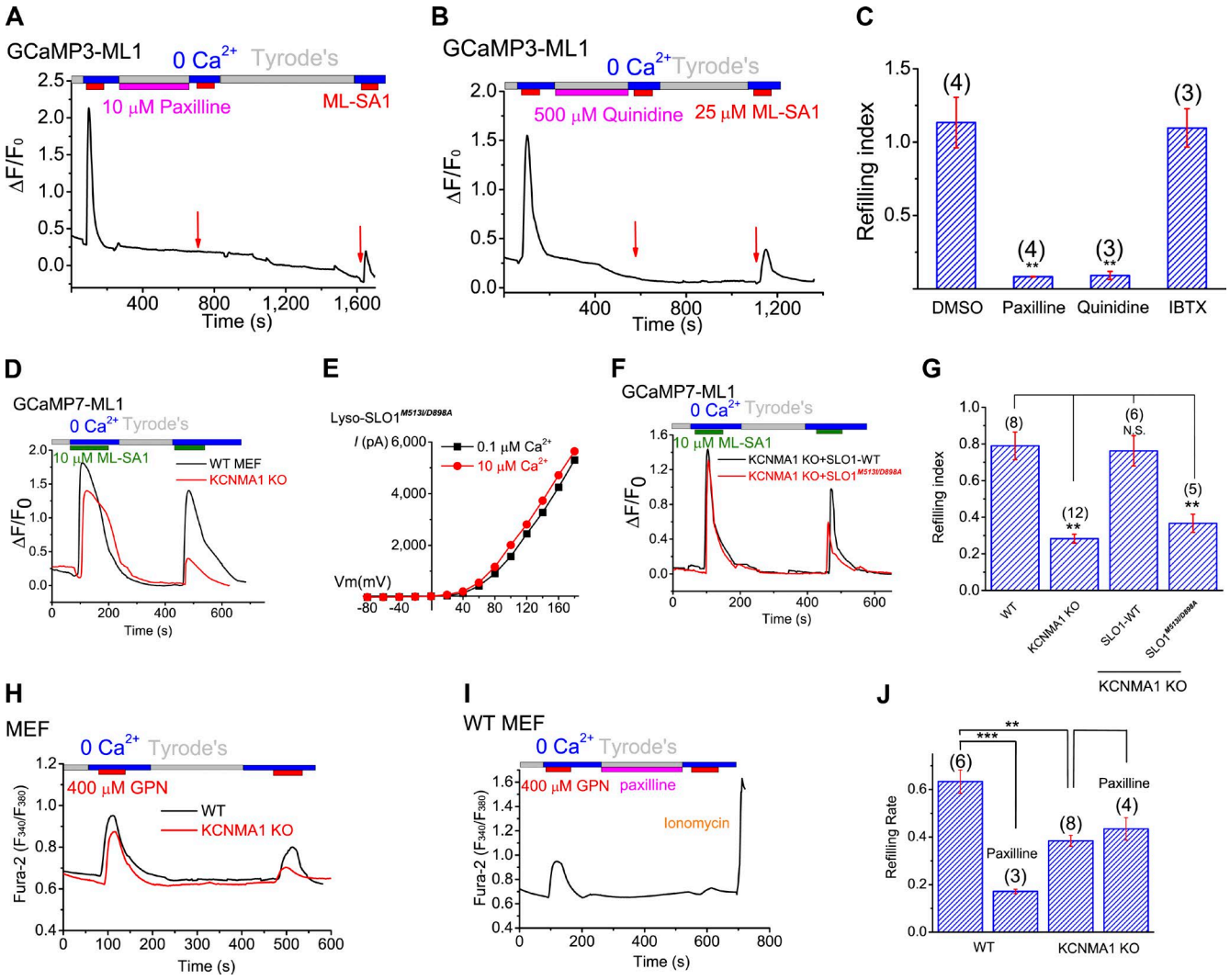

Figure 7. **LysoK$_{VCa}$ and its Ca^{2+} sensitivity regulate the refilling of lysosomal Ca^{2+} stores.** (A and B) Acute application of paxilline (A) and quinidine (B) abolished the second ML-SA1-induced responses. Prolonged washout for 10–15 min led to a partial recovery of the responses. (C) Lysosome Ca^{2+} refilling in HEK-GCaMP3-ML1 cells treated with paxilline, quinidine, and IBTX. (D) Compared with WT MEFs, ML-SA1–stimulated refilled responses were reduced in GCaMP7-ML1-expressing KCNMA1 KO MEFs. (E) Lyso-SLO1$^{M513I/D898A}$ currents at different concentrations of Ca^{2+} (0.1 and 10 μM). (F and G) Lysosomal refilling in GCaMP7-ML1–expressing KCNMA1 KO MEFs that were transfected WT SLO-mCherry and SLO1$^{M513I/D898A}$-mCherry. (H) GPN-induced refilled (the second) Ca^{2+} response, measured with Fura-2 imaging, was reduced in KCNMA1 KO MEFs. (I) Paxilline effects in lysosomal refilling in WT MEF cells. (J) Mean refilling responses in WT and KCNMA1 KO MEF cells. Statistical comparisons were made with variance analysis (Student's *t* test). **, P < 0.01; ***, P < 0.001. Error bars indicate SEM.

for the lysosome, is elevated in most lysosomal storage diseases (Medina et al., 2015; Wang et al., 2015; Xu and Ren, 2015). Likewise, LysoTracker staining is also often elevated in LSD cells that yet have normal lysosomal pH (Xu and Ren, 2015). Indeed, both Lamp1 expression and LysoTracker staining were elevated significantly in KCNMA1 KO MEFs relative to WT cells (Fig. 9, A and B), suggestive of an up-regulation of lysosomal biogenesis caused by lysosomal dysfunction. Note that lysosomal pH was normal in KCNMA1 KO cells (Fig. S6 I).

Lysosomal Ca^{2+} signaling is required for the regulation of lysosomal proteolytic activity and cholesterol homeostasis, presumably via the regulation of lysosomal trafficking (Wang et al., 2015). Lysosomal proteolytic activity was measured using an assay that yields red fluorescence according to the proteolytic degradation of DQ-red-BSA, an artificial substrate (Yue et al., 2013). DQ-BSA degradation was found to be enhanced after complete starvation (withdrawal of both serum and amino acids in the culture medium) of Cos-1 cells (Fig. 9 C). Pharmacological inhibition of LysoK$_{VCa}$ using membrane-permeable, but not membrane-impermeable, BK inhibitors resulted in a marked reduction in the starvation-induced enhancement of proteolytic activity (Fig. 9, C and D). Likewise, in KCNMA1 KO MEFs, proteolytic activity was also attenuated (Fig. 9 E), and the remaining activity became resistant to BK inhibition (Fig. 9 E). Lysosomal cholesterol metabolism is regulated by lysosomal Ca^{2+}, and cholesterol accumulation is observed in multiple LSD cells, including ML-IV and NPC cells (Wang et al., 2015; Xu and Ren, 2015). Compared with WT cells, KCNMA1 KO MEFs exhibited mild but significant cholesterol accumulation (Fig. 9, F and G), suggesting that lysosomal BK is required for efficient cholesterol transport in the lysosomes. Collectively, these results suggest that LysoK$_{VCa}$ is required for the normal function of lysosomes.

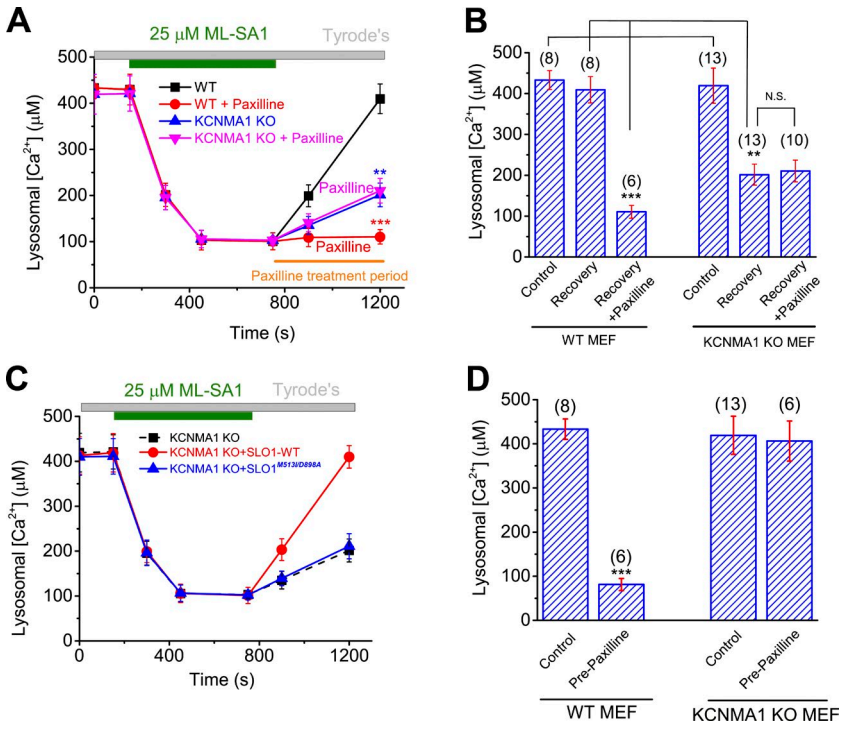

Figure 8. **LysoK$_{VCa}$ is required for the maintenance of lysosomal Ca^{2+} contents.** (A and B) Effects of paxilline on ML-SA1–induced changes in lysosomal Ca^{2+} contents in WT and KCNMA1 KO MEFs. (C) Effects of overexpressing WT SLO-mCherry and SLO1$^{M513I/D898A}$-mCherry on lysosomal Ca^{2+} contents in HEK293 cells. (D) Effects of pretreatment with paxilline on lysosomal Ca^{2+}contents in WT and KCNMA1 KO MEFs. Statistical comparisons were made with variance analysis (Student's *t* test). **, P < 0.01; ***, P < 0.001; N.S., not significant. Error bars indicate SEM.

Discussion

BK channels are negative-feedback regulators of Ca^{2+} overload and membrane hyperexcitability in excitable cells. We demonstrated in the current study that BK channels are functionally present in the lysosomes of both excitable and nonexcitable cells. In contrast, the expression of BK channels at the plasma membrane and early endosomes is absent or very low in the nonexcitable cells. Therefore, BK channels are specifically targeted to the lysosomes, and endogenous SLO1 proteins are bona fide lysosomal channels in many cell types, including MEFs. In another contrast, other plasma membrane background K$^+$ conductances are undetectable in the lysosomes. Using our lysosome-specific Ca^{2+} release and content measurement assays, we showed that lysosomal BK channels are required for efficient refilling of lysosomal Ca^{2+} stores and normal function of lysosomes.

An unexpected finding in the current study is that in the isolated enlarged lysosomes that are used for our electrophysiological measurements, lysosomal $\Delta\psi$ is positive. Our measurement was based on a high $[Na^+]_L/K^+]_L$ ratio previously determined from ionic composition analysis of isolated lysosomes (Wang et al., 2012). If the $[Na^+]_L/K^+]_L$ ratio were lower in intact cells (Steinberg et al., 2010), lysosomal $\Delta\psi$ would be still positive. Several previous studies have reported that lysosomal $\Delta\psi$ are negative, with the values scattered between −10 and −100 mV in different studies and cell types (Morgan et al., 2011). For example, using fluorescence resonance energy transfer–based indicators, one recent study reported that phagolysosomal $\Delta\psi$ is −19 mV in intact single cells (Koivusalo et al., 2011). Recent studies suggest that lysosomal pH is highly heterogeneous, with some of the primary lysosomes completely unacidified (Bright et al., 2016; Johnson et al., 2016). Therefore, our measured lysosomal $\Delta\psi$ based on fixed luminal composition might not be faithfully extrapolated in vivo. It is possible that certain physiological regulators of lysosomal $\Delta\psi$ are lost in our isolated lysosome recordings. However, based on our current study, such unidentified physiological regulators would have to up-regulate lysosomal K$^+$ permeability, as both P_{Na} and P_H contribute to positive $\Delta\psi$.

The vacuolin-1–enlarged vacuoles that we used for patch-clamping most likely originated primarily from late endosomes and lysosomes, as they were positive for Lamp1, but not for ER or mitochondrial markers (Fig. S1 A). Admittedly, the membrane properties of enlarged vacuoles may not be identical to native lysosomal membranes. K_{VCa} currents are undetectable in the early endosomes, and the background and resting K$^+$ conductances at the plasma membrane are also undetectable in the lysosome. Therefore, enlarged endolysosomes do not accumulate any nonlysosomal channel proteins in their limited/perimeter membranes, and the whole-endolysosome technique is reasonably specific in detecting ion channels on the lysosomal membranes. Using this technique, we found that LysoK$_{VCa}$ represents the major K$^+$ conductance in the lysosome, although we estimated based on the single-channel recording data that there are few channels per lysosome (approximately one channel per 1 μm^2 of lysosomal membrane). However, because of the large single-channel conductance, opening of single LysoK$_{VCa}$ currents was sufficient to confer significant changes in lysosomal $\Delta\psi$. Unlike the plasma membrane, in which the opening of ion channels would not significantly change the concentration gradients of ions, opening of LysoK$_{VCa}$ for 100 ms is sufficient to cause the dissipation of the lysosomal K$^+$ gradients. Hence the mean open and close times of single LysoK$_{VCa}$ channels may have large impacts on lysosomal physiology.

It is likely that the primary function of LysoK$_{VCa}$ in lysosomes is to regulate lysosomal $\Delta\psi$, which in turn regulates lysosomal Ca^{2+} refilling and signaling (Fig. 10). In the absence of other major K$^+$ conductances at rest, even with submaximal activation, a brief opening of a single large-conductance K$^+$ channel in the small-sized lysosome can change $\Delta\psi$ rapidly and effectively. During the course of this study, it was reported that

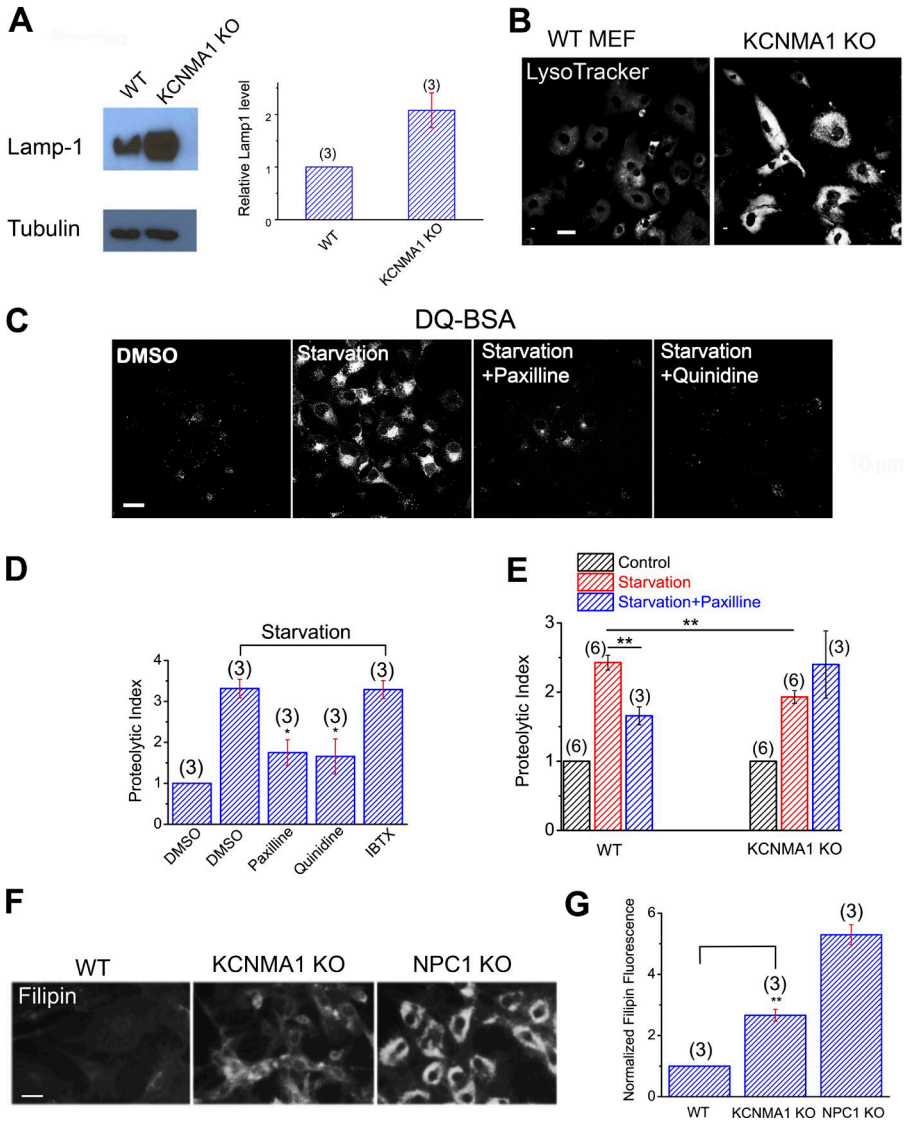

Figure 9. **LysoK$_{VCa}$ is required for lysosome function.** (A) Western blot analysis of Lamp1 expression in WT and KCNMA1 KO MEFs. (B) LysoTracker staining in WT and KCNMA1 KO MEFs. Bar, 10 µm. (C) Confocal imaging of DQ-red-BSA in starved Cos-1 cells (amino acid + serum starvation) in the presence of paxilline (10 µM), quinidine (500 µM), or IBTX (100 nM). Bar, 10 µm. (D) Normalized proteolytic index for starved Cos-1 cells treated with paxilline or quinidine. (E) Normalized proteolytic index for starved WT and KCNMA1 KO MEFs treated with paxilline. (F) Cholesterol levels, detected with filipin staining, in WT, KCNMA1 KO, and NPC1 KO MEFs. Bar, 50 µm. (G) Normalized filipin density in WT, KCNMA1 KO, and NPC1 KO MEFs. Means ± SEM are shown in A, D, E, and G. Statistical comparisons were made using variance analysis (ANOVA for D, E, and G). *, P < 0.05; **, P < 0.01.

TMEM175 proteins may mediate a background K^+ leak conductance. However, this background K^+ current was very small in the original study (20 pA at 100 mV; Cang et al., 2015) and barely detectable in our current experimental conditions. Future studies may reveal the relative contributions of LysoK$_{VCa}$, TMEM175, and other lysosomal K^+ conductances to lysosomal $\Delta\psi$ in various cell types under various cellular conditions. It is important to note that a positive lysosomal $\Delta\psi$ favors the channel openings of LysoK$_{VCa}$ in response to small increases in juxta-lysosomal Ca^{2+} that occur during membrane fusion and fission events. Reversal of $\Delta\psi$ may increase the driving force for ML1-mediated Ca^{2+} release initially, but then deactivate LysoK$_{VCa}$ to shape the duration of lysosomal Ca^{2+} signaling. However, the role of LysoK$_{VCa}$ in lysosomal Ca^{2+} refilling is independent of its effect on lysosomal Ca^{2+} release.

The mechanisms by which the 5,000-fold Ca^{2+} gradient across lysosomal membranes is established and maintained are not clear (Xu and Ren, 2015). We recently reported that the ER serves as a primary source of lysosomal Ca^{2+}, presumably via ER–lysosome membrane contacts (Garrity et al., 2016). However, it remains to be determined how the Ca^{2+} refilling process is triggered. Theoretically, either a reduction in luminal [Ca^{2+}] or an increase of juxta-lysosomal [Ca^{2+}] could trigger the refilling process. In the case of ER Ca^{2+} refilling, STIM proteins mediate luminal Ca^{2+} sensing, and activation of STIM1 triggers the formation of ER–plasma membrane junction and subsequent ORAI channel openings. For lysosomal Ca^{2+} refilling, given that refilling is completely blocked by the chelation of cytoplasmic Ca^{2+}, the latter is more likely the case. However, it is not clear whether Ca^{2+} chelation may affect the formation of ER–lysosome membrane contact sites or the local Ca^{2+} concentrations at the contact sites. Nevertheless, we provide evidence that LysoK$_{VCa}$ could serve as an effector for juxta-lysosomal Ca^{2+}, mediating store refilling. Presumed local Ca^{2+} increases in the ER–lysosome membrane contact sites during the seemingly quiescent refilling phase, but not increases in bulk cytoplasmic Ca^{2+} (e.g., during SERCA inhibition), are required for refilling (Garrity et al., 2016), in which presumed LysoK$_{VCa}$ activation may play a role. However, the mechanisms by which LysoK$_{VCa}$ and $\Delta\psi$ regulate lysosomal Ca^{2+} refilling are unknown, largely because of the lack of the knowledge on the molecular identity of the Ca^{2+} uptake transporters and the regulatory mechanisms of ER–lysosome interaction. Based on our results in the current study, recent studies on ER–lysosome interaction (Phillips and Voeltz, 2016), and previous Ca^{2+} uptake studies on isolated lysosomes (Lemons and Thoene, 1991), we hypothesize that ER

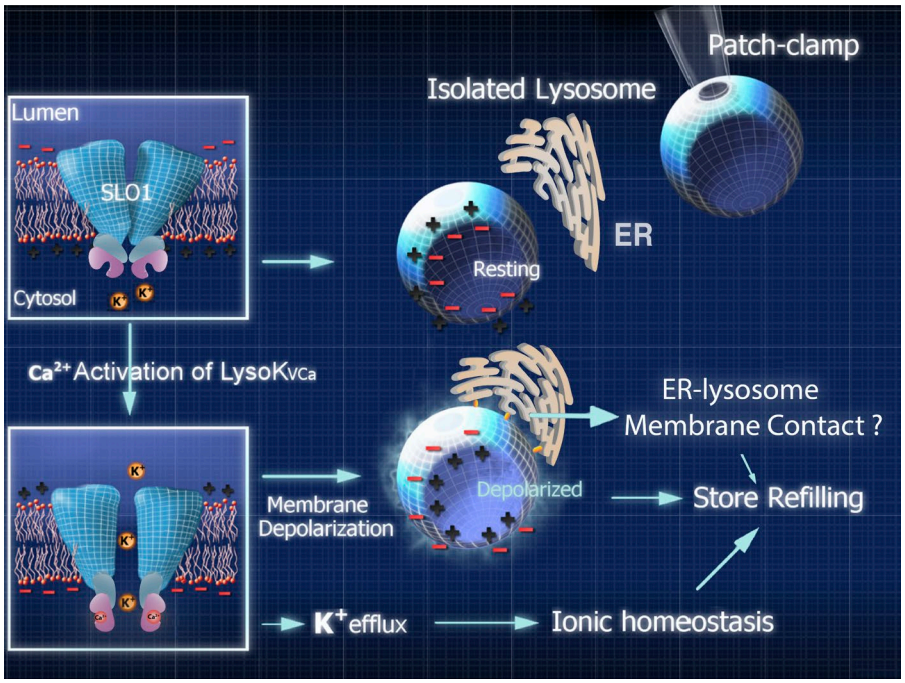

Figure 10. **A working model of the potential roles of LysoK$_{VCa}$-mediated K$^+$ flux in lysosomal dynamics and Ca^{2+} store refilling.** Endolysosomes have a positive Δψ (Fig. 5, A and B) at rest. Upon juxta-lysosomal Ca^{2+} increase, LysoKVCa-mediated K$^+$ flux causes reduction and reversal of Δψ toward E_K (−57 mV, assuming a 10-fold concentration gradient). Changes in lysosomal Δψ may initiate the refilling of lysosomal Ca^{2+} stores via yet-to-be-defined mechanisms, such as formation of ER–lysosome membrane contact sites.

refilling of lysosomal stores is a regulated two-step process. First, lysosome store depletion may trigger an arrangement of ER–lysosome contact configuration (Phillips and Voeltz, 2016). Perilysosomal Ca^{2+} increases were proposed to regulate ER–lysosome membrane contact, but the direct evidence is still lacking (Eden, 2016). Second, at these relatively stable, functional ER–lysosome contact sites, a passive Ca^{2+} transport process can occur from ER to lysosomes, because of the large chemical gradient of Ca^{2+} that is created when lysosome stores are actively depleted. It is conceivable that both steps are dependent on lysosomal Δψ, either directly or indirectly. For example, it is recently reported that Δψ may affect dynamics of phosphoinositide (Zhou et al., 2015), which is known to regulate the interaction of lysosomes with other organelles (Chu et al., 2015). Furthermore, we show that LysoK$_{VCa}$ is required for the lysosomal export of cholesterol, which is known to affect ER–lysosome interaction and the activities of lysosomal channels and transporters (Xu and Ren, 2015). Future studies may reveal whether lysosomal Δψ regulates ER–lysosome interaction or Ca^{2+} uptake mechanisms via cholesterol export and signaling. Testing these hypotheses comprehensively will require expanding our knowledge of transporters and channels in endolysosomal membranes and the development of accurate methods of measuring endolysosomal potentials in intact cells.

Materials and methods

Molecular biology

Mouse SLO1^{R207Q}-YFP, SLO1$^{L1233I/I234A}$, SLO1$^{L488M/I489M/L733V/I734V}$, and SLO1$^{M513I/D898A}$ were generated from mouse SLO1-YFP (a gift from R. Brenner, University of Texas, San Antonio, TX) with the Quick-Change Lightning Site-Direct Mutagenesis kit (Agilent Technologies). GFP-tagged β1, β2, and β4 constructs were provided by T. Hoshi (University of Pennsylvania, Philadelphia, PA). Genetically encoded Ca^{2+} indicator GCaMP3 and GCaMP7 was fused directly to the N terminus of ML1 (GCaMP3-ML1 and GCaMP7-ML1), as described previously (Shen et al., 2012). All constructs were confirmed by sequencing, and protein expression was verified by Western blotting and fluorescence imaging.

Mouse lines

KCNMA1 KO (*Kcnma*$^{-/-}$ or *Slo1*$^{-/-}$) mice were generated and characterized as described previously (Montgomery and Meredith, 2012). All animal experiments were conducted using an approved protocol (#6577) and Institutional Animal Care Guidelines of the University of Michigan.

Mammalian cell culture

Cos-1 cells, HEK-293T cells, CV1 cells, A7r5 cells, and BECs were grown at 37°C in a 1:1 mixture of DMEM supplemented with 10% FBS (Gibco) in a humidified 5% CO_2 incubator. INS-1 cells were cultured in RPMI-1640 (11 mM glucose) supplemented with 10% FBS and 50 mM β-mercaptoethanol. HEK293 cells stably expressing GCaMP3-ML1 (HEK-GCaMP3-ML1 cells) were generated using the Flip-In T-Rex 293 cell line (Invitrogen). HEK-GCaMP3-ML1 cells were grown in Tet-free FBS, and GCaMP3-ML1 expression was induced using doxycycline.

MEF isolation

Sterilized skin specimens from WT and KCNMA1 KO mice were minced into small fragments (~1 mm^2) and incubated in 0.05% trypsin and 0.2% collagenase at 37°C for 1 h. Single fibroblasts, isolated by repeated pipetting, were maintained in DMEM supplemented with 20% FBS and an antibiotic and antimycotic cocktail (Thermo Fisher Scientific) at 37°C in a 5% CO_2 incubator.

Primary cortical neurons

Mouse pups were killed within 2 d of birth, and brains were dissected in ice-cold HBSS. After the removal of meninges, the dissected brains were minced into small fragments (~1 mm^3). Tissue fragments were then incubated in 0.05% trypsin at 37°C for 1 h. Cortical neurons were isolated mechanically by repeated pipetting and plated on poly-L-lysine–coated glass coverslips. Cultures were maintained in a neurobasal medium containing B27 supplement (1×), GlutaMAX (1×), and antibiotic cocktail (100 U/ml penicillin, 100 mg/ml streptomycin, and 0.25

mg/ml fungizone) at 37°C in 5% CO_2. Whole-endolysosomal recordings were performed in neurons that were cultured for more than 10 d.

Lysosome isolation by subcellular fractionation

Lysosomes were isolated as described previously (Wang et al., 2012). In brief, cell lysates were obtained by Dounce homogenization in a homogenizing buffer (HM buffer: 0.25 M sucrose, 1 mM EDTA, and 10 mM Hepes, pH 7.0). Nuclei and intact cells were removed by centrifugation at 1,900 *g* at 4°C for 10 min. Supernatant was then collected and further centrifuged through a Percoll density gradient using a Beckman L8-70 centrifuge and a 70.1 Ti rotor. The Percoll gradient was prepared with 0.7 ml of 2.5 M sucrose at the bottom, 6 ml of 18% Percoll (mixture of 1.08 ml Percoll and 4.92 ml HM buffer) in the middle, and 1 ml postnuclear supernatants on the top. The centrifuge was performed at 4°C for 1 h at 67,200 *g* (14,000 rpm). Heavy membrane fractions containing lysosomes were concentrated at the bottom of the Percoll gradient. They were carefully collected and laid over a discontinuous iodixanol gradient. The centrifuge tube was loaded with 0.5 ml of 2.5 M sucrose at the bottom, and the iodixanol gradient was generated through dilution of iodixanol (by HM buffer) to a final vol/vol (from bottom of the centrifuge tube to top) of 27, 22.5, 19, 16, 12, and 8%. The heavy membrane fraction (1 ml) was laid carefully on top, and the fractionation was performed at 130,000 *g* (44,200 rpm) for 2.5 h at 4°C. After fractionation, the sample was carefully divided into fractions of 0.5 ml. Fractions containing the highest purity of lysosomes were determined using Western blotting and used for subsequent analysis.

Western blotting

Standard Western blotting procedures were used. In brief, cells were lysed with ice-cold RIPA buffer (Boston BioProducts) in the presence of 1× protease inhibitor cocktail (Sigma-Aldrich), 1 mM NaF, and 1 mM Na_3VO_4. Total cell lysates were mixed with 2× SDS loading buffer and boiled at 95°C for 10 min. Protein samples (10–100 µg) were then loaded and separated on 4–12% gradient SDS-PAGE gels (Invitrogen) and transferred to PVDF membranes. The membranes were blocked for 1 h with 1% BSA in PBS supplemented with 0.1% Tween20 and incubated with antibodies against GFP (1:10,000; Covance), Lamp1 (1:1,000; Developmental Studies Hybridoma Bank), EEA1 (1:1,000; Santa Cruz Biotechnology, Inc.), and Complex II (1:1,000; Abcam). Bound antibodies were detected using HRP-conjugated anti-rabbit (65-6120) or anti-mouse (62-6520) secondary antibodies (1:5,000; Invitrogen) and enhanced chemiluminescence reagent (GE Healthcare). Band intensities were quantified with ImageJ software.

Immunofluorescent labeling and confocal imaging

Cells were grown on glass coverslips, fixed with 4% PFA, and permeabilized with 0.3% Triton X-100. They were then blocked with 1% BSA in PBS. After three washes with PBS, the slides with Fluoromount-G (SouthernBiotech) were processed for imaging using a confocal microscope (TCS SP5; Leica Biosystems) with a 100× oil objective NA 1.40 (HCX PL APO; Leica Biosystems). PMT detector was used for DAPI signal (excitation, 405 nm; emission, 410–440 nm); HyD detector was used for GFP (excitation, 488 nm; emission, 492–535 nm) and mCherry/Alexa Fluor 568 (excitation, 561 nm; emission, 575–625nm) signals. Images were acquired with LAS AF software (Leica Biosystems) and analyzed with ImageJ and Photoshop CS6 (Adobe).

GCaMP3-Ca^{2+} imaging

Tet-On HEK-GCaMP3-ML1 stable cells were used for Ca^{2+} imaging. Doxycycline (0.01 µg/ml) was applied 20–24 h before the experiments to induce GCaMP3-ML1 expression. Cells were trypsinized and plated on coverslips 4–6 h before experiments. GCaMP3 fluorescence intensity at 470 nm (F_{470}) was monitored and recorded at RT (21–23°C) using a EasyRatio Pro system (Photon Technology International), which includes an invert microscope (Olympus 1X71) with a 20×/0.75 objective lens (Olympus UApo/340), a high-resolution CoolSNAP HQ^2 CCD camera (Photometrics), and a high-speed DeltaRam X monochromator (Photon Technology International) operated with EasyRatioPro software 1.12.121.86 (Photon Technology International). During recording, cells were bathed in Tyrode's solution containing 145 mM NaCl, 5 mM KCl, 2 mM $CaCl_2$, 1 mM $MgCl_2$, 10 mM glucose, and 20 mM Hepes, pH 7.4. Lysosomal Ca^{2+} release was measured by briefly switching to a 0 Ca^{2+} solution, which contained 145 mM NaCl, 5 mM KCl, 3 mM $MgCl_2$, 10 mM glucose, 1 mM EGTA, and 20 mM Hepes, pH 7.4; free Ca^{2+} concentration is estimated to be <10 nM based on Maxchelator software (Shen et al., 2012). Alterations of Ca^{2+} levels were normalized and shown as $\Delta F/F_0$, where F_0 is baseline F, and ΔF is changes in F upon treatment.

OG-BAPTA imaging

Cells were loaded with OG-BAPTAn (100 µg/ml; Thermo Fisher Scientific) at 37°C in the culture medium for 4–12 h, and then pulsed/chased for additional 4–16 h. Fluorescence imaging was performed at 37°C with a Spinning Disc Confocal Imaging System, which includes an IX81 inverted microscope (Olympus), a 60× oil objective NA 1.42 (Olympus; PlanApo N), a CSU-X1 scanner (Yokogawa Electric Corporation), and an iXon EM-CCD camera (Andor). Images were acquired and analyzed with MetaMorph Advanced Imaging acquisition software v. 7.7.8.0 (Molecular Devices). In vitro calcium-binding (K_d) affinities of OG-BAPTA were determined using KCl-based solutions (140 mM KCl, *x* mM $CaCl_2$, 1 mM $MgCl_2$, 10 mM Hepes, 10 mM MES, and 0 or 1 mM BAPTA) adjusted to different pH levels (4.5, 5.0, 6.0, and 7.0). By varying the amount of added Ca^{2+} (x = 0–10 mM), solutions with different pH and free [Ca^{2+}] were made based on Maxchelator software. OG-BAPTA (5 µg/ml) fluorescence for each solution was obtained to plot the calibration curve (Christensen et al., 2002; Dickson et al., 2012; Morgan et al., 2015). In cells that were pretreated with ionomycin, nigericin, and valinomycin, in vivo minimal and maximal fluorescence (F_{min} and F_{max}) were determined by perfusing the cells with 0 or 10 mM Ca^{2+} external solutions, respectively (Christensen et al., 2002; Dickson et al., 2012; Morgan et al., 2015). Lysosomal [Ca^{2+}] were at different pH were determined using the following calibration equation: $[Ca^{2+}] = K_d \times (F - F_{min})/(F_{max} - F)$.

Lysosomal pH measurement

Cells seeded on coverslips were pulsed with OG-BAPTA (100 µg/ml) at 37°C in the culture medium for 6 h and chased for additional 12 h (Johnson et al., 2016). Cells were then bathed in Tyrode's solution. Images were captured at RT using an EasyRatio Pro system (Photon Technology International). Fluorescence was continuously recorded at RT with alternated excitation wavelengths of 480 and 430 nm (F_{480} and F_{430}, respectively). To convert fluorescence ratios (F_{480}/F_{430}) to pH values, a pH standard curve was constructed using isotonic K^+ solutions (145 mM KCl, 5 mM glucose, 1 mM $MgCl_2$, 1 mM $CaCl_2$, 10 mM Hepes, and 10 mM MES, adjusted to various pH values ranging from 4.0 to 8.0) containing 10 µM nigericin and 10 µM monensin (Johnson et al., 2016).

Whole-endolysosome electrophysiology

Endolysosomal electrophysiology was performed on isolated endolysosomes using a modified patch-clamp method (Dong et al., 2008). In brief, cells were treated with 1 µM vacuolin-1, a lipid-soluble polycyclic triazine that can increase the size of endosomes and lysosomes selectively (Cerny et al., 2004), for at least 1 h and up to 12 h. Large vacuoles

(up to 5 µm in diameter; capacitance = 1.9 ± 0.1 pF, n = 35 vacuoles) were observed in most vacuolin-treated cells. Occasionally, enlarged vacuoles were also seen in nontreated cells; no significant difference in $LysoK_{VCa}$ channel properties were seen for enlarged vacuoles obtained with or without vacuolin-1 treatment (Fig. S1 B). To isolate vacuoles, a patch pipette (electrode) was pressed against individual cells and then pulled away quickly to sever the cell membrane. Whole-endolysosome recordings were then performed on enlarged vacuoles from cells that were released into the dish. Note that the membrane properties of enlarged vacuoles may not be identical to native lysosomal membranes. However, the whole-endolysosome technique is thus far the only feasible approach for directly studying lysosomal channels (Xu and Ren, 2015).

Unless otherwise stated, the bath (internal/cytoplasmic) solution contained 140 mM K^+-gluconate, 4 mM NaCl, 2 mM $MgCl_2$, and 10 mM Hepes (pH adjusted with KOH to 7.2). Solutions with 0.1–10 µM free Ca^{2+} were prepared by combining various concentrations of EGTA and $CaCl_2$, as calculated with Maxchelator. Bath solutions with 100–1,000 µM Ca^{2+} contained various amounts of $CaCl_2$ without EGTA. pH adjustments (6.0, 7.2, and 9.0) were made in either 0.1 µM Ca^{2+} internal solution with 1 mM EGTA or 100 µM Ca^{2+} internal solution without EGTA. The pipette (luminal) solution contained 145 mM NaCl, 5 mM KCl, 2 mM $CaCl_2$, 1 mM $MgCl_2$, 10 mM Hepes, 10 mM MES, and 10 mM glucose (pH adjusted to 4.6 with NaOH). To avoid contamination of background Cl^- currents existing in some patches, low-Cl^- pipette solutions were used in many experiments, in which Na-gluconate was used as a substitute for NaCl. All bath solutions were applied via a fast perfusion system to achieve a complete solution exchange within a few seconds. Data were acquired with an Axopatch 2A patch-clamp amplifier and a Digidata 1440 digitizer and recorded with pClamp 10.0 software (Axon Instruments). Whole-endolysosome currents were digitized at 10 kHz and filtered at 2 kHz. All experiments were conducted at RT (21–23°C), and all recordings were analyzed in pCLAMP10 (Axon Instruments) and Origin 8.0 (OriginLab) software.

Endolysosomal excised-patch electrophysiology

For giant excised-patch, endolysosomal luminal-side-out recordings, polished pipette electrodes (resistance, 1–2 MΩ) were filled with a solution containing 140 mM K^+-gluconate, 4 mM NaCl, 2 mM $MgCl_2$, 1 mM $CaCl_2$, and 10 mM Hepes (pH adjusted with KOH to 7.2). The bath solution contained 153 mM NaCl, 5 mM KCl, 2 mM $CaCl_2$, 1 mM $MgCl_2$, 20 mM Hepes, and 10 mM glucose, pH 7.4. Excised-patch, endolysosomal cytoplasmic-side-out (Dong et al., 2008) recordings were performed in isolated enlarged endolysosomes with the same pipette and bath solutions that were used in the whole-endolysosome recordings.

Whole-cell electrophysiology

Whole-cell recordings were performed in Cos-1 cells via pipette electrodes (resistance 3–5 MΩ) filled with the following solution: 140 mM K^+-gluconate, 4 mM NaCl, 2 mM $MgCl_2$, 0.1 mM $CaCl_2$ (unless otherwise indicated), and 10 mM Hepes (pH adjusted with KOH to 7.2). The standard extracellular bath solution (modified Tyrode's solution) contained 153 mM NaCl, 5 mM KCl, 2 mM $CaCl_2$, 1 mM $MgCl_2$, 10 mM Hepes, 10 mM MES, and 10 mM glucose (pH adjusted to 4.6 with NaOH). Data were acquired with an Axopatch 2A patch-clamp amplifier and a Digidata 1440 digitizer and recorded with pClamp software.

DQ-BSA proteolytic assay

DQ-red-BSA was used as an artificial substrate to evaluate lysosomal proteolytic degradation (Yue et al., 2013). In brief, cells were treated with DQ-red-BSA (10 µg/ml; Thermo Fisher Scientific) for 2 h at 37°C in complete culture medium. After removal of extracellular DQ-red-BSA by washing twice with PBS, cells were starved in amino acid– and serum-free DF12 medium (US Biological) for 2 h to trigger autophagic degradation. To examine the effects of BK blockers on lysosomal proteolytic activities, paxilline (10 µM), quinidine (500 µM), or IBTX (100 nM) was applied during starvation. Cells were then fixed with 4% PFA for 15 min at RT, washed twice with PBS, and mounted on slides with Fluoromount-G (SouthernBiotech). DQ-red-BSA fluorescence was detected with a 561/607 filter set using the Spinning Disc Confocal Imaging System under an 60× oil objective NA 1.42 (Olympus; PlanApo N). Images were acquired and analyzed with MetaMorph Advanced Imaging acquisition software v. 7.7.8.0 (Molecular Devices). Quantification was performed using ImageJ.

Filipin staining

Cells were fixed in 4% PFA for 1 h, washed three times with PBS, and then incubated with 1.5 mg/ml glycine in PBS for 10 min to quench the PFA. Cells were then stained for 2 h with 0.05 mg/ml filipin in PBS supplemented with 10% FBS. All procedures were conducted at RT (21–23°C). Images were obtained using a fluorescence microscope with a UV filter. Filipin intensity was calculated using ImageJ.

Reagents

All reagents were dissolved and stored in DMSO or water. DQ-BSA-red was from Life Technologies; anti-SLO-1 antibodies were purchased from NeuroMab; vacuolin-1 was from Calbiochem; ML-SA1 was from Princeton BioMolecular Research Inc.; quinidine, paxilline, clofilium tosylate, NS1619, IBTX, TEA chloride, and filipin complex were purchased from Sigma-Aldrich.

Data analysis

Data are presented as mean ± SEM. Statistical comparisons were performed using Student's t test and analysis of variance (ANOVA). P-values <0.05 were considered statistically significant.

Online supplemental material

Fig. S1 shows that vacuolin-1 selectively enlarges endosomes and lysosomes. Fig. S2 shows that $LysoK_{VCa}$ currents are present in a variety of cell types. Fig. S3 shows the regulation of $LysoK_{VCa}$ by Ca^{2+}, Mg^{2+}, and membrane voltages. Fig. S4 shows the regulation of $LysoK_{VCa}$ by BK modulators and pH. Fig. S5 shows cell type–specific properties of $LysoK_{VCa}$ conferred by lysosomal localization of auxiliary β subunits. Fig. S6 shows the regulation of lysosomal Ca^{2+} refilling by $LysoK_{VCa}$.

Acknowledgments

We are grateful to Drs. Robert Brenner, Jianming Cui (Washington University), and Fumitaka Kudo (Tokyo Institute of Technology) for sharing the reagents, as well as to former laboratory members Drs. Xianping Dong and Xiang Wang for their pilot studies on Ca^{2+}-activated conductances in lysosomes. We appreciate the encouragement and helpful comments from other members of the Xu laboratory.

This work was supported by National Institutes of Health grants NS062792 and AR060837 (to H. Xu) and HL102758 (to A. Meredith).

The authors declare no competing financial interests.

Author contributions: W. Wang conceived, designed, and performed the electrophysiology and Ca^{2+} imaging experiments; W. Wang and H. Xu drafted the manuscript with inputs from all authors; X. Zhang and M. Gu performed electrophysiological experiments; Q. Gao performed the proteolytic assay; M. Lawas performed the Ca^{2+} imaging experiments; Q. Gao, L. Yu, and X. Cheng performed the confocal imaging experiments; N. Sahoo and X. Li performed the biochemistry experiments; S. Ireland and A. Meredith provided reagents; H. Xu supervised the project.

Submitted: 16 December 2016
Revised: 5 March 2017
Accepted: 10 April 2017

References

Bandyopadhyay, D., A. Cyphersmith, J.A. Zapata, Y.J. Kim, and C.K. Payne. 2014. Lysosome transport as a function of lysosome diameter. *PLoS One.* 9:e86847. http://dx.doi.org/10.1371/journal.pone.0086847

Bao, L., C. Kaldany, E.C. Holmstrand, and D.H. Cox. 2004. Mapping the BKCa channel's 'Ca2+ bowl': Side-chains essential for Ca2+ sensing. *J. Gen. Physiol.* 123:475–489. http://dx.doi.org/10.1085/jgp.200409052

Berg, T.O., E. Strømhaug, T. Løvdal, O. Seglen, and T. Berg. 1994. Use of glycyl-L-phenylalanine 2-naphthylamide, a lysosome-disrupting cathepsin C substrate, to distinguish between lysosomes and prelysosomal endocytic vacuoles. *Biochem. J.* 300:229–236. http://dx.doi.org/10.1042/bj3000229

Braun, M., R. Ramracheya, M. Bengtsson, Q. Zhang, J. Karanauskaite, C. Partridge, P.R. Johnson, and P. Rorsman. 2008. Voltage-gated ion channels in human pancreatic beta-cells: Electrophysiological characterization and role in insulin secretion. *Diabetes.* 57:1618–1628. http://dx.doi.org/10.2337/db07-0991

Bright, N.A., L.J. Davis, and J.P. Luzio. 2016. Endolysosomes are the principal intracellular sites of acid hydrolase activity. *Curr. Biol.* 26:2233–2245. http://dx.doi.org/10.1016/j.cub.2016.06.046

Cai, X., Y. Xu, Y.M. Kim, J. Loureiro, and Q. Huang. 2014. PIKfyve, a class III lipid kinase, is required for TLR-induced type I IFN production via modulation of ATF3. *J. Immunol.* 192:3383–3389. http://dx.doi.org/10.4049/jimmunol.1302411

Cang, C., K. Aranda, Y.J. Seo, B. Gasnier, and D. Ren. 2015. TMEM175 is an organelle K(+) channel regulating lysosomal function. *Cell.* 162:1101–1112. http://dx.doi.org/10.1016/j.cell.2015.08.002

Cao, Q., X.Z. Zhong, Y. Zou, Z. Zhang, L. Toro, and X.P. Dong. 2015. BK channels alleviate lysosomal storage diseases by providing positive feedback regulation of lysosomal Ca2+ release. *Dev. Cell.* 33:427–441. http://dx.doi.org/10.1016/j.devcel.2015.04.010

Cerny, J., Y. Feng, A. Yu, K. Miyake, B. Borgonovo, J. Klumperman, J. Meldolesi, P.L. McNeil, and T. Kirchhausen. 2004. The small chemical vacuolin-1 inhibits Ca(2+)-dependent lysosomal exocytosis but not cell resealing. *EMBO Rep.* 5:883–888. http://dx.doi.org/10.1038/sj.embor.7400243

Christensen, K.A., J.T. Myers, and J.A. Swanson. 2002. pH-dependent regulation of lysosomal calcium in macrophages. *J. Cell Sci.* 115:599–607.

Chu, B.B., Y.C. Liao, W. Qi, C. Xie, X. Du, J. Wang, H. Yang, H.H. Miao, B.L. Li, and B.L. Song. 2015. Cholesterol transport through lysosome-peroxisome membrane contacts. *Cell.* 161:291–306. http://dx.doi.org/10.1016/j.cell.2015.02.019

Dickson, E.J., J.G. Duman, M.W. Moody, L. Chen, and B. Hille. 2012. Orai-STIM-mediated Ca2+ release from secretory granules revealed by a targeted Ca2+ and pH probe. *Proc. Natl. Acad. Sci. USA.* 109:E3539–E3548. http://dx.doi.org/10.1073/pnas.1218247109

Dong, X.P., X. Cheng, E. Mills, M. Delling, F. Wang, T. Kurz, and H. Xu. 2008. The type IV mucolipidosis-associated protein TRPML1 is an endolysosomal iron release channel. *Nature.* 455:992–996. http://dx.doi.org/10.1038/nature07311

Dong, X.P., D. Shen, X. Wang, T. Dawson, X. Li, Q. Zhang, X. Cheng, Y. Zhang, L.S. Weisman, M. Delling, and H. Xu. 2010. PI(3,5)P(2) controls membrane trafficking by direct activation of mucolipin Ca(2+) release channels in the endolysosome. *Nat. Commun.* 1:38. http://dx.doi.org/10.1038/ncomms1037

Eden, E.R. 2016. The formation and function of ER-endosome membrane contact sites. *Biochim. Biophys. Acta.* 1861(8, 8 Pt B):874–879. http://dx.doi.org/10.1016/j.bbalip.2016.01.020

Fonseca, B.D., G.H. Diering, M.A. Bidinosti, K. Dalal, T. Alain, A.D. Balgi, R. Forestieri, M. Nodwell, C.V. Rajadurai, C. Gunaratnam, et al. 2012. Structure-activity analysis of niclosamide reveals potential role for cytoplasmic pH in control of mammalian target of rapamycin complex 1 (mTORC1) signaling. *J. Biol. Chem.* 287:17530–17545. http://dx.doi.org/10.1074/jbc.M112.359638

Garrity, A.G., W. Wang, C.M. Collier, S.A. Levey, Q. Gao, and H. Xu. 2016. The endoplasmic reticulum, not the pH gradient, drives calcium refilling of lysosomes. *eLife.* 5:15887. http://dx.doi.org/10.7554/eLife.15887

Hoshi, T., Y. Tian, R. Xu, S.H. Heinemann, and S. Hou. 2013. Mechanism of the modulation of BK potassium channel complexes with different auxiliary subunit compositions by the omega-3 fatty acid DHA. *Proc. Natl. Acad. Sci. USA.* 110:4822–4827. http://dx.doi.org/10.1073/pnas.1222003110

Johnson, D.E., P. Ostrowski, V. Jaumouillé, and S. Grinstein. 2016. The position of lysosomes within the cell determines their luminal pH. *J. Cell Biol.* 212:677–692. http://dx.doi.org/10.1083/jcb.201507112

Kilpatrick, B.S., E.R. Eden, L.N. Hockey, E. Yates, C.E. Futter, and S. Patel. 2017. An endosomal NAADP-sensitive two-pore Ca(2+) channel regulates ER-endosome membrane contact sites to control growth factor signaling. *Cell Reports.* 18:1636–1645. http://dx.doi.org/10.1016/j.celrep.2017.01.052

Kiselyov, K., S. Yamaguchi, C.W. Lyons, and S. Muallem. 2010. Aberrant Ca2+ handling in lysosomal storage disorders. *Cell Calcium.* 47:103–111. http://dx.doi.org/10.1016/j.ceca.2009.12.007

Koivusalo, M., B.E. Steinberg, D. Mason, and S. Grinstein. 2011. In situ measurement of the electrical potential across the lysosomal membrane using FRET. *Traffic.* 12:972–982. http://dx.doi.org/10.1111/j.1600-0854.2011.01215.x

Lemons, R.M., and J.G. Thoene. 1991. Mediated calcium transport by isolated human fibroblast lysosomes. *J. Biol. Chem.* 266:14378–14382.

Li, B., W. Jie, L. Huang, P. Wei, S. Li, Z. Luo, A.K. Friedman, A.L. Meredith, M.H. Han, X.H. Zhu, and T.M. Gao. 2014. Nuclear BK channels regulate gene expression via the control of nuclear calcium signaling. *Nat. Neurosci.* 17:1055–1063. http://dx.doi.org/10.1038/nn.3744

Liu, J., J. Ye, X. Zou, Z. Xu, Y. Feng, X. Zou, Z. Chen, Y. Li, and Y. Cang. 2014. CRL4A(CRBN) E3 ubiquitin ligase restricts BK channel activity and prevents epileptogenesis. *Nat. Commun.* 5:3924.

Medina, D.L., S. Di Paola, I. Peluso, A. Armani, D. De Stefani, R. Venditti, S. Montefusco, A. Scotto-Rosato, C. Prezioso, A. Forrester, et al. 2015. Lysosomal calcium signalling regulates autophagy through calcineurin and TFEB. *Nat. Cell Biol.* 17:288–299. http://dx.doi.org/10.1038/ncb3114

Mindell, J.A. 2012. Lysosomal acidification mechanisms. *Annu. Rev. Physiol.* 74:69–86. http://dx.doi.org/10.1146/annurev-physiol-012110-142317

Montgomery, J.R., and A.L. Meredith. 2012. Genetic activation of BK currents in vivo generates bidirectional effects on neuronal excitability. *Proc. Natl. Acad. Sci. USA.* 109:18997–19002. http://dx.doi.org/10.1073/pnas.1205573109

Morgan, A.J., F.M. Platt, E. Lloyd-Evans, and A. Galione. 2011. Molecular mechanisms of endolysosomal Ca^{2+} signalling in health and disease. *Biochem. J.* 439:349–374. http://dx.doi.org/10.1042/BJ20110949

Morgan, A.J., L.C. Davis, and A. Galione. 2015. Imaging approaches to measuring lysosomal calcium. *Methods Cell Biol.* 126:159–195. http://dx.doi.org/10.1016/bs.mcb.2014.10.031

Nishiyama, Y., T. Ohmichi, S. Kazami, H. Iwasaki, K. Mano, Y. Nagumo, F. Kudo, S. Ichikawa, Y. Iwabuchi, N. Kanoh, et al. 2016. Vicenistatin induces early endosome-derived vacuole formation in mammalian cells. *Biosci. Biotechnol. Biochem.* 80:902–910. http://dx.doi.org/10.1080/09168451.2015.1132152

Olesen, S.P., E. Munch, P. Moldt, and J. Drejer. 1994. Selective activation of Ca(2+)-dependent K+ channels by novel benzimidazolone. *Eur. J. Pharmacol.* 251:53–59. http://dx.doi.org/10.1016/0014-2999(94)90442-1

Patel, S. 2015. Function and dysfunction of two-pore channels. *Sci. Signal.* 8:re7. http://dx.doi.org/10.1126/scisignal.aab3314

Phillips, M.J., and G.K. Voeltz. 2016. Structure and function of ER membrane contact sites with other organelles. *Nat. Rev. Mol. Cell Biol.* 17:69–82. http://dx.doi.org/10.1038/nrm.2015.8

Salkoff, L., A. Butler, G. Ferreira, C. Santi, and A. Wei. 2006. High-conductance potassium channels of the SLO family. *Nat. Rev. Neurosci.* 7:921–931. http://dx.doi.org/10.1038/nrn1992

Shen, D., X. Wang, X. Li, X. Zhang, Z. Yao, S. Dibble, X.P. Dong, T. Yu, A.P. Lieberman, H.D. Showalter, and H. Xu. 2012. Lipid storage disorders block lysosomal trafficking by inhibiting a TRP channel and lysosomal calcium release. *Nat. Commun.* 3:731. http://dx.doi.org/10.1038/ncomms1735

Shi, J., G. Krishnamoorthy, Y. Yang, L. Hu, N. Chaturvedi, D. Harilal, J. Qin, and J. Cui. 2002. Mechanism of magnesium activation of calcium-activated potassium channels. *Nature.* 418:876–880. http://dx.doi.org/10.1038/nature00941

Singh, H., E. Stefani, and L. Toro. 2012. Intracellular BK(Ca; iBK(Ca)) channels. *J. Physiol.* 590:5937–5947. http://dx.doi.org/10.1113/jphysiol.2011.215533

Singh, H., R. Lu, J.C. Bopassa, A.L. Meredith, E. Stefani, and L. Toro. 2013. mitoBK(Ca) is encoded by the Kcnma1 gene, and a splicing sequence defines its mitochondrial location. *Proc. Natl. Acad. Sci. USA.* 110:18024. http://dx.doi.org/10.1073/pnas.1302028110

Steinberg, B.E., K.K. Huynh, A. Brodovitch, S. Jabs, T. Stauber, T.J. Jentsch, and S. Grinstein. 2010. A cation counterflux supports lysosomal acidification. *J. Cell Biol.* 189:1171–1186. http://dx.doi.org/10.1083/jcb.200911083

Tang, Q.Y., Z. Zhang, X.M. Xia, and C.J. Lingle. 2010. Block of mouse Slo1 and Slo3 K+ channels by CTX, IbTX, TEA, 4-AP and quinidine. *Channels (Austin).* 4:22–41. http://dx.doi.org/10.4161/chan.4.1.10481

Torres, Y.P., S.T. Granados, and R. Latorre. 2014. Pharmacological consequences of the coexpression of BK channel α and auxiliary β subunits. *Front. Physiol.* 5:383. http://dx.doi.org/10.3389/fphys.2014.00383

Van Dyke, R.W. 1995. Na+/H+ exchange modulates acidification of early rat liver endocytic vesicles. *Am. J. Physiol.* 269:C943–C954.

Wang, W., Q. Gao, M. Yang, X. Zhang, L. Yu, M. Lawas, X. Li, M. Bryant-Genevier, N.T. Southall, J. Marugan, et al. 2015. Up-regulation of lysosomal TRPML1 channels is essential for lysosomal adaptation to nutrient starvation. *Proc. Natl. Acad. Sci. USA.* 112:E1373–E1381. http://dx.doi.org/10.1073/pnas.1419669112

Wang, X., X. Zhang, X.P. Dong, M. Samie, X. Li, X. Cheng, A. Goschka, D. Shen, Y. Zhou, J. Harlow, et al. 2012. TPC proteins are phosphoinositide-activated sodium-selective ion channels in endosomes and lysosomes. *Cell.* 151:372–383. http://dx.doi.org/10.1016/j.cell.2012.08.036

Wegner, C.S., L. Malerød, N.M. Pedersen, C. Progida, O. Bakke, H. Stenmark, and A. Brech. 2010. Ultrastructural characterization of giant endosomes induced by GTPase-deficient Rab5. *Histochem. Cell Biol.* 133:41–55. http://dx.doi.org/10.1007/s00418-009-0643-8

Xia, X.M., J.P. Ding, and C.J. Lingle. 2003. Inactivation of BK channels by the NH2 terminus of the beta2 auxiliary subunit: An essential role of a terminal peptide segment of three hydrophobic residues. *J. Gen. Physiol.* 121:125–148. http://dx.doi.org/10.1085/jgp.20028667

Xu, H., and D. Ren. 2015. Lysosomal physiology. *Annu. Rev. Physiol.* 77:57–80. http://dx.doi.org/10.1146/annurev-physiol-021014-071649

Yamamura, H., Y. Ohi, K. Muraki, M. Watanabe, and Y. Imaizumi. 2001. BK channel activation by NS-1619 is partially mediated by intracellular Ca2+ release in smooth muscle cells of porcine coronary artery. *Br. J. Pharmacol.* 132:828–834. http://dx.doi.org/10.1038/sj.bjp.0703885

Yan, J., and R.W. Aldrich. 2010. LRRC26 auxiliary protein allows BK channel activation at resting voltage without calcium. *Nature.* 466:513–516. http://dx.doi.org/10.1038/nature09162

Yang, H., J. Shi, G. Zhang, J. Yang, K. Delaloye, and J. Cui. 2008. Activation of Slo1 BK channels by Mg2+ coordinated between the voltage sensor and RCK1 domains. *Nat. Struct. Mol. Biol.* 15:1152–1159. http://dx.doi.org/10.1038/nsmb.1507

Yuan, P., M.D. Leonetti, A.R. Pico, Y. Hsiung, and R. MacKinnon. 2010. Structure of the human BK channel Ca2+-activation apparatus at 3.0 A resolution. *Science.* 329:182–186. http://dx.doi.org/10.1126/science.1190414

Yue, W., A. Hamaï, G. Tonelli, C. Bauvy, V. Nicolas, H. Tharinger, P. Codogno, and M. Mehrpour. 2013. Inhibition of the autophagic flux by salinomycin in breast cancer stem-like/progenitor cells interferes with their maintenance. *Autophagy.* 9:714–729. http://dx.doi.org/10.4161/auto.23997

Zeng, X.H., J.P. Ding, X.M. Xia, and C.J. Lingle. 2001. Gating properties conferred on BK channels by the beta3b auxiliary subunit in the absence of its NH(2)- and COOH termini. *J. Gen. Physiol.* 117:607–628. http://dx.doi.org/10.1085/jgp.117.6.607

Zhou, Y., C.O. Wong, K.J. Cho, D. van der Hoeven, H. Liang, D.P. Thakur, J. Luo, M. Babic, K.E. Zinsmaier, M.X. Zhu, et al. 2015. Membrane potential modulates plasma membrane phospholipid dynamics and K-Ras signaling. *Science.* 349:873–876. http://dx.doi.org/10.1126/science.aaa5619